

Engineering Research Express



OPEN ACCESS

PAPER

Analytical modeling of an inclined folded-beam spring used in micromechanical resonator devices

RECEIVED
20 January 2023REVISED
17 March 2023ACCEPTED FOR PUBLICATION
28 June 2023PUBLISHED
14 July 2023**Ahmad Rahbar Ranji** **, Andy Li, Shahpour Alirezaee and Mohammad Jalal Ahamed**

Department of Mechanical, Automotive and Material Engineering, University of Windsor, Windsor, Canada

E-mail: ranji@uwindsor.ca**Keywords:** crab length spring, finite element method, folded beam spring, MEMS, principal axes of spring constant, serpentine spring, ANSYS

Original content from this work may be used under the terms of the [Creative Commons Attribution 4.0 licence](#).

Any further distribution of this work must maintain attribution to the author(s) and the title of the work, journal citation and DOI.

**Abstract**

Accurate estimation of the mechanical behavior of springs is crucial for the proper design of Microelectromechanical systems (MEMS). The main objective of this study is to derive a closed-form equation for the calculation of the stiffness of an inclined spring in the form of folded-beams. The energy-based method was used to calculate the displacements of a folded-beams that was fixed at one end and glued at the other end. The analytical model was then compared with the finite element method using ANSYS for different inclination angles of the folded-beams spring, showing good agreement. The angle of inclination has changed from zero to 180 degrees, and stiffness of folded-beams is determined. The derived expressions of the compliances were checked for the case of serpentine springs with inclination angle of zero, and different length ratios against the literature. It is found that neglecting small lengths for calculating the stiffness of the folded-beams spring is not justified. The influential geometrical parameters, including different lengths of the spring and inclination angle of the spring, on the stiffness are studied. It is found that the angle of inclination of the principal axes of spring constants depends on the geometrical parameters, and the angle of inclination has more effect on the stiffness of a folded-beams spring than the number of folds.

Nomenclature

Symbol	Definition
α	Direction that folded-beams spring is free to displace, or Angle of inclination of folded-beams spring.
β	Direction perpendicular to angle of inclination of folded-beams spring.
$\delta_\alpha, \delta_\beta$	Displacement of the spring in α , and β directions
C_{ij}	Compliance coefficient in i direction due to unit load in j direction
F_α, F_β	Applied loads in α , and β directions
$I_{ini}, I_{fin}, I_p, I_0$	Moment of Inertia of different parts of a folded-beam spring
$l_{ini}, l_{fin}, l_p, l_0$	Length of different parts of a folded-beam spring
k_α, k_β	Spring constant in α , and β directions
$k_{\alpha\beta}$	Cross axis spring constant
k_1, k_2	Principal spring constant

1. Introduction

Many different types of springs are used in Microelectromechanical systems (MEMS) based inertial devices [1]. MEMS inertial devices are used as accelerometers in the automotive industry, gyroscopes as inertial navigation

systems, piezoelectric vibration and pressure sensors, MEMS switches, timing devices, resonators, strain gauges, and fiber optic sensors. Potential applications of springs are diverse and include MEMS actuators, MEMS XY stage, RF switches, and energy harvesting devices [2]. The main functions of the springs in these devices are reduction of vibration, keeping elements in position, connection between elements, and application of repulsive force [2].

Among various MEMS inertial devices, an accelerometer is a device that senses the inertial reaction of a proof mass for the purpose of measuring linear or angular acceleration [3] and is used in automotive, biomedical, robotics, consumer, and military industries [4]. It is composed of a proof mass in the form of a rectangular plate suspended via beams (springs) to a fixed frame, whose displacement is proportional to the acceleration it receives [5]. The proof mass displaces with respect to the external frame due to the applied acceleration, which in turn causes contraction/extension of the supporting springs. Both displacement of the proof mass and induced force in the springs are used to measure the applied acceleration [6]. Generally, all micromachined accelerometers are modeled as a mass-spring-damper system [4]. One performance parameter of the accelerometer is the Q-factor (quality factor), which is related to the ratio of stored energy to dissipated energy. The quality factor of the accelerometer is defined as:

$$Q = \frac{\sqrt{Mk}}{D} \quad (1)$$

where M is the mass of the proof mass, k is the spring constant of the suspension beams, and D is the damping coefficient. To manipulate the quality factor, where the mass is fixed, the spring stiffness and damping should be tuned to achieve the desired Q-factor. Another important parameter for accelerometers is their sensitivity. The ratio of the proof mass displacement to the applied acceleration is defined as the static sensitivity of an accelerometer. To increase the sensitivity of an accelerometer, the ratio of the proof mass to the supporting beam stiffness should be increased [7]. The total noise equivalent acceleration (TNEA) is calculated as [8, 9]:

$$TNEA = \frac{\sqrt{4K_B TD}}{M} \quad (2)$$

where K_B is the Boltzmann constant ($1.38 \times 10^{-23} J/K$), T is the absolute temperature in kelvin, D is the viscous damping coefficient, and M is the proof mass of an accelerometer. To reduce the noise, the proof mass should be increased and have the damping reduced. Thus, in general, the damping of the accelerometers should be minimal, and the proof mass should be maximal. However, the stiffness should be a trade-off between the quality and static sensitivity. Accurate estimation of the spring constant is therefore crucial and one of the most complicated aspects of vibration analysis.

The accelerometer can be a single-axis (single-degree of freedom) accelerometer, in which the proof mass is free to displace in one direction. In this case, the suspended beam can be one beam in the form of a cantilever beam [10], two suspended beams in the form of a double cantilever beam [11], two beams at the middle of the two parallel edges of the proof mass called a simple bridge or four beams at the corner of two parallel edges called a double bridge (also known as clamped-clamped flexure [12]). To increase the flexibility of the accelerometers, the straight beams are folded, and to have symmetry, they are used at four corners of the proof mass called folded-beam and crab-leg beams [12]. The suspension beam has also been used in the form of an in-plane frame around the proof mass and parallel to the fixed frame [13].

Another type of MEMS inertial sensor that uses a vibratory proof mass supported by springs is a gyroscope. A MEMS gyroscope is a vibratory gyroscope [14] in which a vibratory element in place of a traditional spinning element [15] is used to measure angular rotation or angular velocity with Coriolis effects [1]. The vibratory element or proof mass can be in the form of a beam, plate or shell suspended by flexible beams above a substrate [16]. The simplified equation of motion of MEMS vibratory gyroscopes is based on a spring-mass-damper system [17], which can be based on linear or torsional motion [16]. In linear MEMS gyroscopes, the proof mass should be free to vibrate in two orthogonal linear directions, in which the supporting beams are in the form of crab-leg, serpentine, U-shape, and frame [18–20]. The gyroscopes have a pair of principal elastic axes that define stable directions of a straight-line motion of the gyroscope [21]. If the principal spring constant is defined as k_1 and k_2 , the stiffness of the spring in the general direction is defined as [22]:

$$\begin{cases} k_\alpha = \frac{k_1 + k_2}{2} + \frac{k_1 - k_2}{2} \cos 2\theta \\ k_\beta = \frac{k_1 + k_2}{2} - \frac{k_1 - k_2}{2} \cos 2\theta \\ k_{\alpha\beta} = \frac{k_1 - k_2}{2} \sin 2\theta \end{cases} \quad (3)$$

where θ is the angle between the principal axis and α axis, and $k_{\alpha\beta}$ is the cross-axis stiffness of the spring. Mounting the spring on its principal axes eliminates any cross-axis motion. Appropriately mounting springs in the principal axes can affect the performance of MEMS by reducing parasitic motion, increasing the quality factor, and eliminating cross-axis motion.

Reducing the actuation voltage of MEMS switches broadens the range of their application and enhances their application [23]. Among the different methods, lowering the switch spring constant is the best approach to reduce the actuation voltage [23, 24]. Selection of the spring in the MEMS depends on the fabrication process, size limitation and, most importantly, stiffness. The folded-beamss are chosen due to their low value of stiffness in a restricted area [25]. Saffari *et al* [26] introduced a rotated serpentine spring to reduce the stiffness and actuation voltage of RF MEMS. Folded-beam springs are also used in MEMS optical switches due to their high reliability [27].

Fedder [12] analytically calculated the spring constants of a serpentine spring using the energy method. Iyer *et al* [28] used the energy method to derive the spring constant of U-spring, crab-leg and serpentine spring. Barrilaro *et al* [29] calculated the torsional stiffness of a serpentine spring using the energy method. Lu *et al* [30] proposed an expression for the calculation of the stiffness of classical and rotated serpentine springs. Wai-Chi *et al* [31] and Witter and Howell [32] determined the stiffness of a U-shape spring considering shear deformation. Liu and Wen [33] gave an equation for the calculation of a folded-beam spring. Urey *et al* [34] calculated the stiffness constant of flexural beams for five different modes of vibration used in micromechanical scanners. Kovacs and Vizvary [35] compared the sensitivity of an accelerometer with cantilever and bridge-type springs. Grandos-Rojas *et al* [36] optimized the number of folded-beams to have the required stiffness of the spring within the available space. Jiang *et al* [37] compared two spring configurations of folded-beams and coild springs from the point of view of having the same stiffness in both directions while occupying less area. Xia *et al* [38] used different types of folded-beam springs in a tri-axis linear vibratory gyroscope and adjusting the springs' dimensions minimized the frequency mismatches between different modes of vibration. Zhou and Dowd [39] proposed a tilted folded-beam spring for comb-drive actuators. Rouabah *et al* [40] numerically compared the stiffnesses of square and curved serpentine springs for out-of-plane motion in an electrostatic actuator MEMS. Kaya *et al* [41] and Petsch and Kaya [42] numerically studied the dynamic behavior of serpentine springs with variable lengths mounted at 45 degrees in an accelerometer. Yamane *et al* [43] analyzed the spring constant of a serpentine beam in the z direction to suspend the high-density proof mass of an accelerometer. Guo *et al* [44] determined the stiffness of a curve serpentine spring in the form of an S-shape in a three-axis gyroscope.

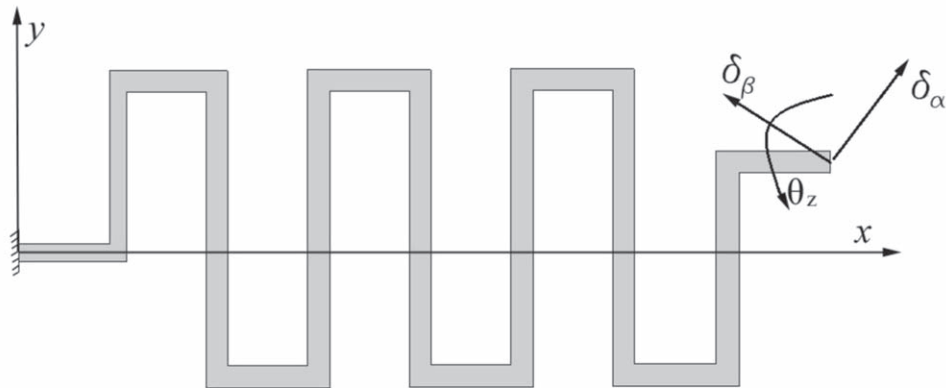
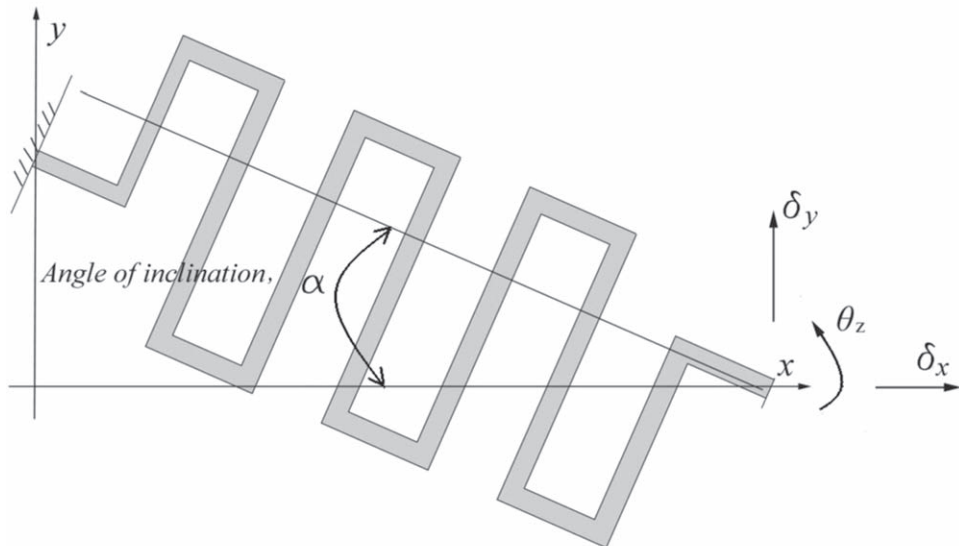
The quality factor, stability and sensitivity of MEMS resonators depend on the stiffness of the springs. However, depending on the type of MEMS, the stiffness should be maximum or minimum, and in most cases, it is desirable to have minimum stiffness in one direction and maximum stiffness in the orthogonal direction [45]. Stiffness calculations of folded-beam springs have been used for years in MEMS resonators; however, stiffness of folded-beam springs in a general direction never received detailed attention in the literature. Advance manufacturing methods make it possible to use incline springs for better performance and optimize the use of resticted space. In addition, due to fabrication errors, the stiffness matrix would not be diagonal, and nondiagonal terms cause coupling of motion in two orthogonal directions, leading to quadrature error for the drive mode in gyroscopes [46, 47]. Thus, it is necessary to have the spring constant of folded-beam springs in a general direction of motion to determine the principal axes of stiffness.

Research on vibration and spring performance is interdisciplinary and involves fields such as electrical, mechanical, and material science. The main aim of the present study is to use the energy method to derive the spring constant of a folded-beam when it is free to dispalce in any direction. A literature-based equation and finite element method (FEM) are used to validate the derived expressionBy mounting a spring in an inclination angle to achieve benefits that go beyond what is possible with conventional arrangements. In the next section, the energy method is used to calculate the stiffness of a general folded-beam spring, followed by the numerical method. In section four, the stiffness of different types of folded-beam springs, including serpentine spring, U-shape spring, and crab-length beams, are determined and discussed for different inclination angles, and in section five, the conclusions are given.

2. Stiffness analysis of a folded-beam free to displace in a general direction

The serpentine and crab-leg springs consist of folded-beams with rectangular cross sections (figure 1).

In micromechanical chips, one end of the springs is fixed to the surrounding frame, and the other end is connected to the proof mass, which can displace with the proof mass in any direction. For an inclined spring and/or when the proof mass moves in any direction, it is necessary to have the spring constant of this spring in a general direction. Energy-based Castiglano's method used to derive the displacement of a folded-beam spring. The bending moments, $M(x)$ at all parts are calculated ([appendix](#)), and the displacements of the free end of the

(a) Horizontal folded-beam spring free to displace in α , and β direction.(b) Inclined folded-beam spring free to displace in x , and y directions.**Figure 1.** A folded-beam spring fixed at one end and free to displace at the other end.

folded-beam are calculated as follows:

$$\delta_\alpha = \int_s \frac{M(x) \frac{\partial M(x)}{\partial F_\alpha}}{EI} dx \quad (4)$$

$$\delta_\beta = \int_s \frac{M(x) \frac{\partial M(x)}{\partial F_\beta}}{EI} dx \quad (5)$$

$$\theta_z = \int_s \frac{M(x) \frac{\partial M(x)}{\partial M_\theta}}{EI} dx \quad (6)$$

where δ_α and δ_β are displacements of the spring at the free end in the α and β directions, respectively θ_z is the rotation of the free end around the z axis (figure 1), F_α and F_β are the applied forces at the free end in the α and β directions, respectively, M_θ is the applied bending moment around the z -axis at the free end, and EI is flexural rigidity of folded-beam.

Substituting the bending moment from the appendix in equations (4)–(6) yields the following relations for calculating the displacements:

$$\delta_\alpha = F_\alpha C_{\alpha\alpha} + F_\beta C_{\beta\beta} + M_\theta C_{\alpha\theta} \quad (7)$$

$$\delta_\beta = F_\alpha C_{\beta\alpha} + F_\beta C_{\beta\beta} + M_\theta C_{\beta\theta} \quad (8)$$

$$\theta_z = F_\alpha C_{\theta\alpha} + F_\beta C_{\theta\beta} + M_\theta C_{\theta\theta} \quad (9)$$

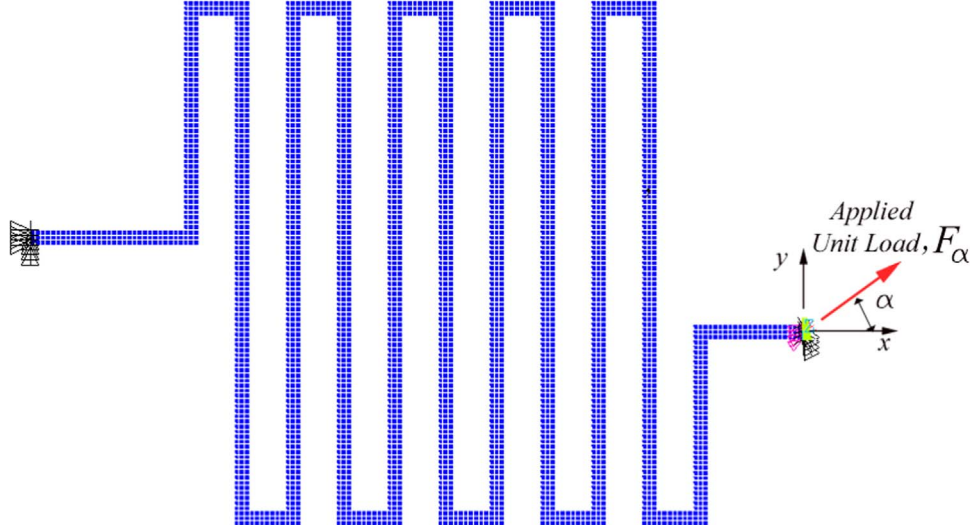


Figure 2. Finite element model of a folded-beam spring fixed at one end and free to displace in α direction at the other end.

Equations (7)–(9) can be expressed as follows:

$$\begin{bmatrix} \delta_\alpha \\ \delta_\beta \\ \theta_z \end{bmatrix} = \begin{bmatrix} C_{\alpha\alpha} & C_{\alpha\beta} & C_{\alpha\theta} \\ C_{\beta\alpha} & C_{\beta\beta} & C_{\beta\theta} \\ C_{\theta\alpha} & C_{\theta\beta} & C_{\theta\theta} \end{bmatrix} \begin{bmatrix} F_\alpha \\ F_\beta \\ M_\theta \end{bmatrix} \quad (10)$$

where C_{ij} are the compliance coefficients of the folded-beam spring and are given in the [appendix](#). Thus, the stiffness of the spring in the α and β directions is defined as:

$$k_\alpha = \frac{C_{\beta\beta} \times C_{\theta\theta} - C_{\theta\beta} \times C_{\beta\theta}}{\begin{vmatrix} C_{\alpha\alpha} & C_{\alpha\beta} & C_{\alpha\theta} \\ C_{\beta\alpha} & C_{\beta\beta} & C_{\beta\theta} \\ C_{\theta\alpha} & C_{\theta\beta} & C_{\theta\theta} \end{vmatrix}} \quad (11)$$

$$k_\beta = \frac{C_{\alpha\alpha} \times C_{\theta\theta} - C_{\theta\alpha} \times C_{\alpha\theta}}{\begin{vmatrix} C_{\alpha\alpha} & C_{\alpha\beta} & C_{\alpha\theta} \\ C_{\beta\alpha} & C_{\beta\beta} & C_{\beta\theta} \\ C_{\theta\alpha} & C_{\theta\beta} & C_{\theta\theta} \end{vmatrix}} \quad (12)$$

$$k_{\alpha\beta} = k_{\beta\alpha} = \frac{C_{\alpha\beta} \times C_{\theta\theta} - C_{\theta\beta} \times C_{\alpha\theta}}{\begin{vmatrix} C_{\alpha\alpha} & C_{\alpha\beta} & C_{\alpha\theta} \\ C_{\beta\alpha} & C_{\beta\beta} & C_{\beta\theta} \\ C_{\theta\alpha} & C_{\theta\beta} & C_{\theta\theta} \end{vmatrix}} \quad (13)$$

3. Numerical method

To validate the results of equations (11)–(13), the finite element simulation software, ANSYS v.2022 R [48] was used using solid elements, solid185, which has eight nodes with three degrees of freedom at each node, and translations in the nodal x , y , and z directions (figure 2).

A fixed boundary condition at one end is imposed by restraining all degrees of freedom of all nodes. The other end is free to move only in the direction of α ; thus, degrees of freedom in the direction of β and rotation around z -axis are restrained, and in the direction of α , all nodes are coupled. Young's modulus is selected as $1.60 \times 10^{11} \text{ Pa}$, and Poisson's ratio is selected as 0.22. A unit load is applied in the direction of α , and the displacement in this direction is determined.

4. Results and discussion

The equations of the compliances ([appendix](#)) are used to investigate the effect of different geometrical parameters, including the number of folds, the ratio of the length of connector beams to span beams, and the ratio of end beams to span beams, on the stiffness of the inclined folded-beams. To demonstrate the applicability of the method, the stiffness of serpentine springs with two different lengths of first and last span beams are determined and compared with available equations in the literature, followed by U-shape springs and crab-length springs.

4.1. Inclined serpentine spring with, $l_1 = l_2 = 0.5 l_0$, $I_{ini} = I_{fin}$, and $l_{ini} = l_{fin}$

In a serpentine spring, the length of connector beams, l_p is smaller than length of span beams, l_0 . For the case of, $l_1 = l_2 = 0.5 l_0$, $I_{ini} = I_{fin}$, and $l_{ini} = l_{fin}$ ([figure 3](#)), the compliance equations given in the [appendix](#) for the calculation of the stiffness of an inclined serpentine spring are simplified as follows:

$$\begin{aligned}
 C_{\alpha\alpha}/\frac{(l_0)^3}{EI_0} &= \frac{1}{6}(m+1)(\cos\alpha)^2 + \frac{1}{4}(m+1)\frac{l_p}{l_0}\sin 2\alpha + (m+1)\left[2\frac{l_{fin}}{l_0}\left(\frac{l_{fin}}{l_0} + 2(m+1)\frac{l_p}{l_0}\right)\right. \\
 &\quad \left. + \left(\frac{8}{3}m^2 + \frac{16}{3}m + 3\right)\left(\frac{l_p}{l_0}\right)^2\right](\sin\alpha)^2 + (m+1)\frac{l_p}{l_0}\frac{I_0}{I_p}\left\{\frac{1}{2}(\cos\alpha)^2 + \frac{1}{2}\frac{l_p}{l_0}\sin 2\alpha\right. \\
 &\quad \left.+ 2\left[\left(\frac{l_{fin}}{l_0}\right)^2 + 2(m+1)\frac{l_p}{l_0}\left(\frac{l_{fin}}{l_0} + \frac{2}{3}(m+1)\frac{l_p}{l_0}\right)\right](\sin\alpha)^2\right\} \\
 &\quad + \frac{I_0}{I_{fin}}\frac{l_{fin}}{l_0}\left[\frac{8}{3}\left(\frac{l_{fin}}{l_0}\right)^2 + 6(m+1)\frac{l_p}{l_0}\left(\frac{l_{fin}}{l_0} + \frac{2}{3}(m+1)\frac{l_p}{l_0}\right)\right](\sin\alpha)^2 \\
 C_{\alpha\beta}/\frac{(l_0)^3}{EI_0} &= C_{\beta\alpha}/\frac{(l_0)^3}{EI_0} = (m+1)\left[-\frac{1}{12} + \frac{l_{fin}}{l_0}\left(\frac{l_{fin}}{l_0} + 2(m+1)\frac{l_p}{l_0}\right) + \left(\frac{4}{3}m^2 + \frac{8}{3}m + \frac{3}{2}\right)\left(\frac{l_p}{l_0}\right)^2\right]\sin 2\alpha \\
 &\quad + \frac{1}{4}(m+1)\frac{l_p}{l_0}\cos 2\alpha + (m+1)\frac{l_p}{l_0}\frac{I_0}{I_p}\left[\left(-\frac{1}{4} + \left(\frac{l_{fin}}{l_0}\right)^2 + 2(m+1)\frac{l_p}{l_0}\left(\frac{l_{fin}}{l_0} + \frac{2}{3}(m+1)\frac{l_p}{l_0}\right)\right)\sin 2\alpha\right. \\
 &\quad \left.+ \frac{1}{2}\frac{l_p}{l_0}\cos 2\alpha\right] + \frac{I_0}{I_{fin}}\frac{l_{fin}}{l_0}\left[\frac{8}{6}\left(\frac{l_{fin}}{l_0}\right)^2 + 3(m+1)\frac{l_p}{l_0}\left(\frac{l_{fin}}{l_0} + \frac{2}{3}(m+1)\frac{l_p}{l_0}\right)\right]\sin 2\alpha \\
 C_{\beta\beta}/\frac{(l_0)^3}{EI_0} &= \frac{1}{6}(m+1)(\sin\alpha)^2 - \frac{1}{4}(m+1)\frac{l_p}{l_0}\sin 2\alpha + \\
 &\quad (m+1)\left(2\frac{l_{fin}}{l_0}\left(\frac{l_{fin}}{l_0} + 2(m+1)\frac{l_p}{l_0}\right) + \left(\frac{8}{3}m^2 + \frac{16}{3}m + 3\right)\left(\frac{l_p}{l_0}\right)^2\right)(\cos\alpha)^2 \\
 &\quad + (m+1)\frac{I_0}{I_p}\frac{l_p}{l_0}\left[\frac{1}{2}(\sin\alpha)^2 - \frac{1}{2}\frac{l_p}{l_0}\sin 2\alpha\right. \\
 &\quad \left.+ 2\left(\left(\frac{l_{fin}}{l_0}\right)^2 + 2(m+1)\frac{l_p}{l_0}\left(\frac{l_{fin}}{l_0} + \frac{2}{3}(m+1)\frac{l_p}{l_0}\right)\right)(\cos\alpha)^2\right] \\
 &\quad + \frac{I_0}{I_{fin}}\frac{l_{fin}}{l_0}\left[\frac{8}{3}\left(\frac{l_{fin}}{l_0}\right)^2 + 6(m+1)\frac{l_p}{l_0}\left(\frac{l_{fin}}{l_0} + \frac{2}{3}(m+1)\frac{l_p}{l_0}\right)\right](\cos\alpha)^2 \\
 C_{\theta\alpha}/\frac{(l_0)^2}{EI_0} &= C_{\alpha\theta}/\frac{(l_0)^2}{EI_0} = 2\left(\frac{l_{fin}}{l_0} + (m+1)\frac{l_p}{l_0}\right)\left((m+1)\left(1 + \frac{I_0}{I_p}\frac{l_p}{l_0}\right) + \frac{I_0}{I_{fin}}\frac{l_{fin}}{l_0}\right)\sin\alpha \\
 C_{\beta\theta}/\frac{(l_0)^2}{EI_0} &= C_{\theta\beta}/\frac{(l_0)^2}{EI_0} = 2\left(\frac{l_{fin}}{l_0} + (m+1)\frac{l_p}{l_0}\right)\left((m+1)\left(1 + \frac{I_0}{I_p}\frac{l_p}{l_0}\right) + \frac{I_0}{I_{fin}}\frac{l_{fin}}{l_0}\right)\cos\alpha \\
 C_{\theta\theta}/\frac{l_0}{EI_0} &= 2(m+1)\left(1 + \frac{I_0}{I_p}\frac{l_p}{l_0}\right) + 2\frac{I_0}{I_{fin}}\frac{l_{fin}}{l_0}
 \end{aligned} \tag{14}$$

As seen, in equation (14), there are many terms with sentences such as $(l_p/l_0)^3$, $(l_{fin}/l_0)^3$, $(l_p/l_0)^2$, $(l_{fin}/l_0)^2$, and $(l_{fin}/l_0)(l_p/l_0)$. To investigate the effect of these terms on the stiffness of the spring, for different values of parameter m , and ratio of $I_{ini} = I_{fin} = I_p = I_0$ the stiffness of the spring as a function of angle α is calculated and depicted in figures 4 and 5.

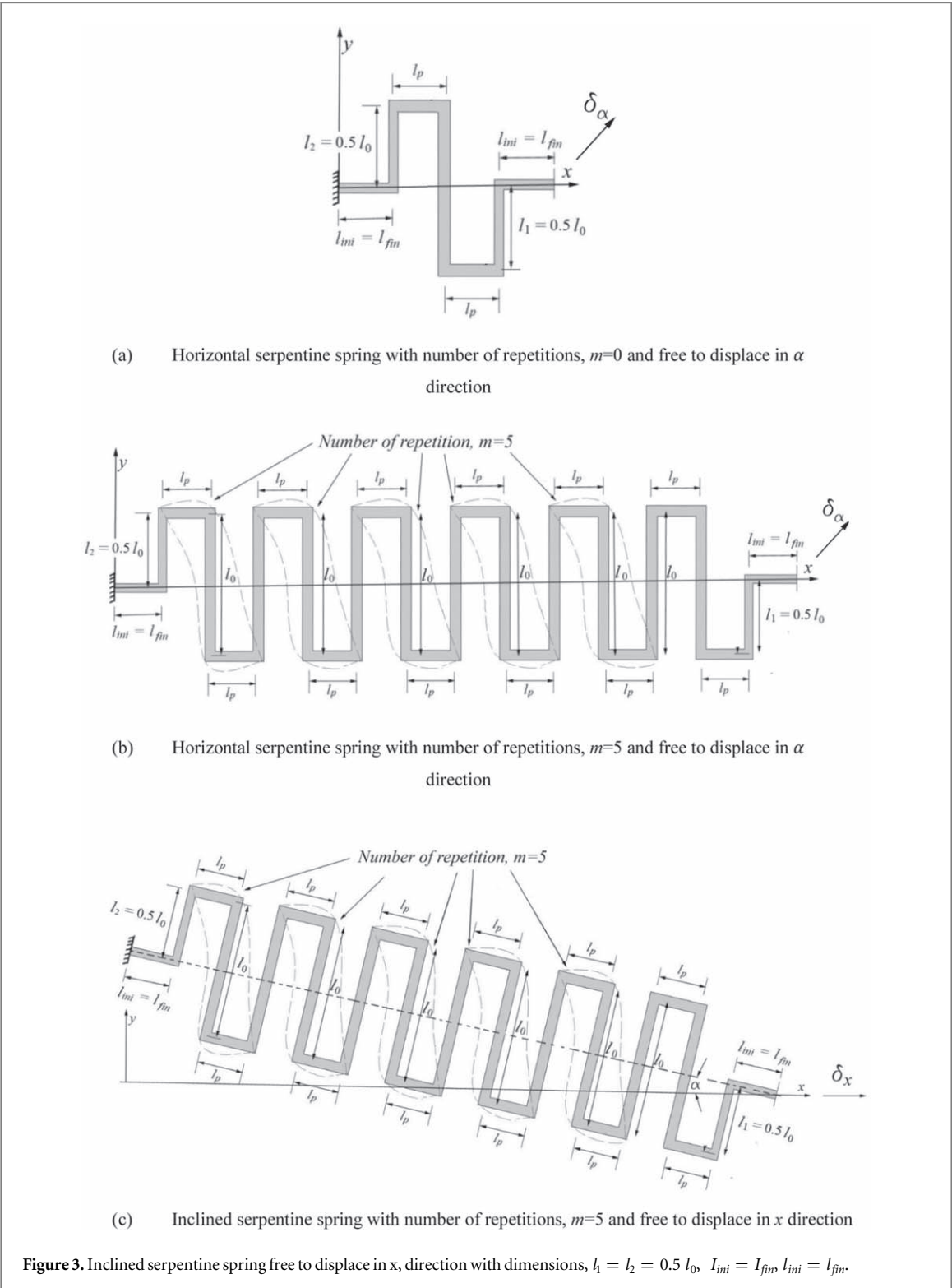


Figure 3. Inclined serpentine spring free to displace in x , direction with dimensions, $l_1 = l_2 = 0.5 l_0$, $l_{ini} = l_{fin}$, $l_{ini} = l_{fin}$.

As seen from figures 4 and 5, for the case of $\alpha = 0$, i.e., $k_\alpha = k_x$ neglecting all values of, $(l_{fin}/l_0)^3$, $(l_p/l_0)^2$, $(l_{fin}/l_0)^2$, and $(l_{fin}/l_0)(l_p/l_0)$ are justified irrespective of the ratio of l_{fin}/l_0 when the parameter m is larger than one. As seen from figure 5(a), for the case of $m = 0$, and $l_p/l_0 = 0.1$, comparing the stiffness of the serpentine spring when all terms are considered and neglecting $(l_p/l_0)^3$, and/or $(l_{fin}/l_0)^3$ yield to 0.4% overestimation of the stiffness, neglecting $(l_p/l_0)^3$, and $(l_p/l_0)^2$ yield to 9% overestimation of the stiffness, and neglecting $(l_p/l_0)^3$, $(l_{fin}/l_0)^3$, $(l_p/l_0)^2$, $(l_{fin}/l_0)^2$, and/or $(l_{fin}/l_0)(l_p/l_0)$ underestimate the stiffness of the spring by 34%. Thus, neglecting only the terms $(l_p/l_0)^3$, and $(l_{fin}/l_0)^3$ are justified.

For inclination angles between 15 and 165 degrees ($k_\alpha \neq k_x$), neglecting $(l_p/l_0)^3$ and $(l_{fin}/l_0)^3$ increases stiffness, and neglecting parameters $(l_p/l_0)^3$,

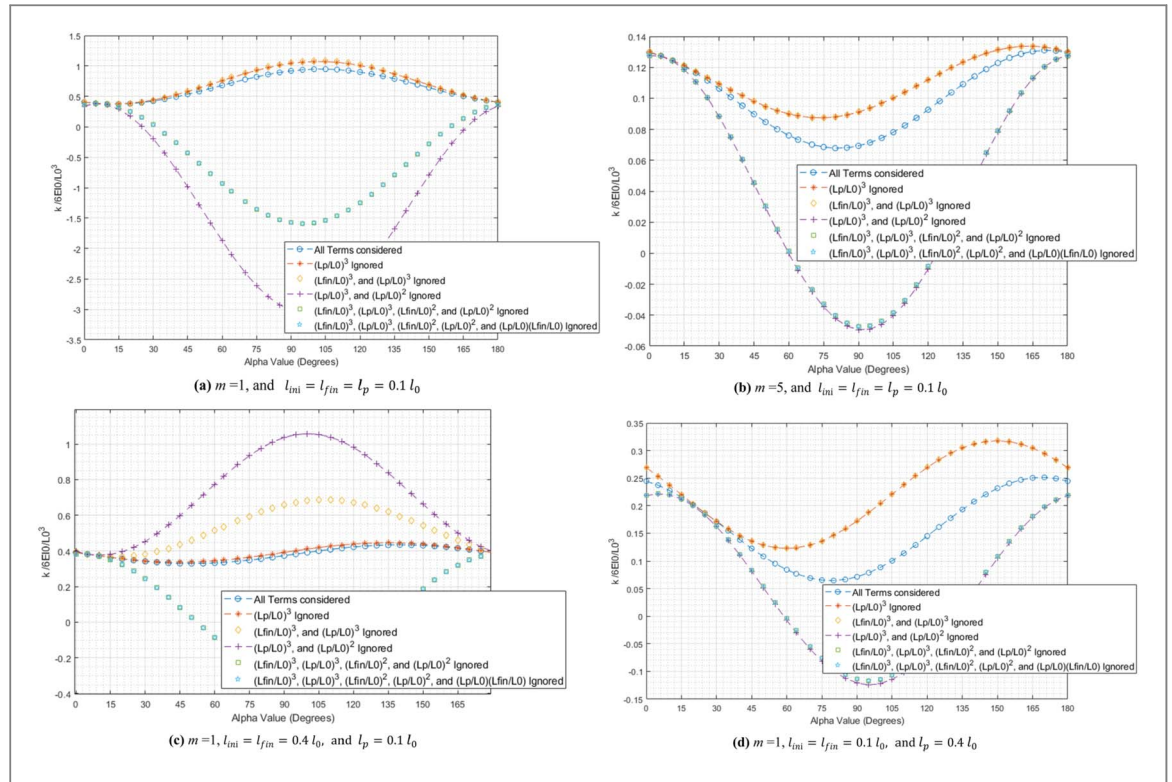


Figure 4. Stiffness of the inclined serpentine spring as a function of inclination angle, α for the case of, $l_1 = l_2 = 0.5 l_0$, and $I_{ini} = I_{fin} = I_p = I_0$.

Table 1. Spring constant of serpentine spring in the x direction, $k_x / \frac{6EI_0}{(l_0)^3}$ for the case of $l_1 = l_2 = 0.5 l_0$ (figure 3), and $I_{ini} = I_{fin} = I_p = I_0$.

Geometrical Parameter	Method	<i>m</i>						
		0	1	2	3	4	5	10
$\frac{l_p}{l_0} = 0.1$	Current Study equation (11)	1.055	0.430	0.271	0.199	0.157	0.130	0.07
	Current study equation (15)	0.664	0.370	0.252	0.190	0.153	0.128	0.07
	Barillaro <i>et al</i> [29]	0.769	0.385	0.256	0.192	0.154	0.128	0.07
$\frac{l_p}{l_0} = 0.2$	FEM	1.063	0.438	0.275	0.201	0.159	0.132	0.07
	Current Study equation (11)	0.915	0.353	0.221	0.162	0.128	0.106	0.057
	Current study equation (15)	0.548	0.302	0.205	0.155	0.124	0.104	0.057
$\frac{l_p}{l_0} = 0.4$	Barillaro <i>et al</i> [29]	0.625	0.313	0.208	0.156	0.125	0.104	0.05
	FEM	0.921	0.358	0.224	0.164	0.129	0.107	0.058
	Current Study equation (11)	0.714	0.259	0.161	0.118	0.093	0.077	0.042
	Current study equation (15)	0.406	0.221	0.150	0.113	0.090	0.076	0.041
	Barillaro <i>et al</i> [29]	0.455	0.227	0.151	0.114	0.091	0.076	0.041
	FEM	0.718	0.261	0.162	0.119	0.094	0.077	0.042

(l_{fin}/l_0)³, (l_p/l_0)², (l_{fin}/l_0)², and (l_{fin}/l_0)(l_p/l_0) yields a negative value for the stiffness of the spring. Thus, for the inclined angle of the spring, even for small values of the length ratio l_p/l_0 and l_{fin}/l_0 neither of these terms should be neglected.

Substituting equation (14) in equation (11) for the case of $\alpha = 0$ and neglecting the length ratio (l_p/l_0)³, (l_p/l_0)³, (l_p/l_0)², (l_{fin}/l_0)², and (l_{fin}/l_0)(l_p/l_0) yields the following relation for calculating the stiffness of a serpentine spring (figure 3) in the x direction, k_x :

$$k_x / \frac{6EI_0}{(l_0)^3} = \frac{(m+1)}{(m+1)^2 \left(1 + 3 \frac{l_0}{l_p} \frac{l_p}{l_0}\right) + \frac{3}{16} \left(1 + \frac{l_0}{l_p} \frac{l_p}{l_0}\right)} \quad (15)$$

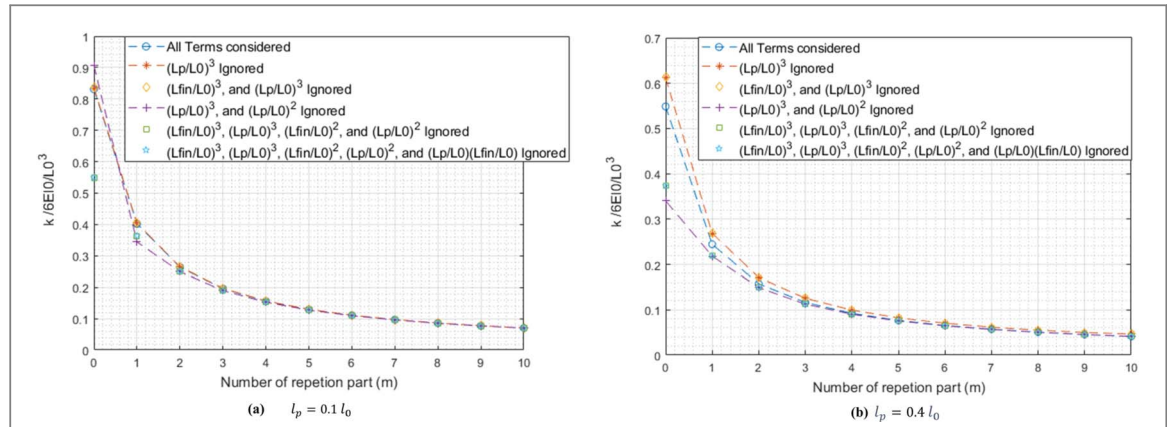


Figure 5. Stiffness of the horizontal serpentine spring ($\alpha = 0$) as a function of number of repetition, m for the case of, $l_1 = l_2 = 0.5 l_0$, $I_{ini} = I_{fin} = I_p = I_0$, and $l_{ini} = l_{fin} = 0.1 l_0$.

Barillaro *et al* [29] have given the following expression for the calculation of k_x :

$$k_x / \left(\frac{6EI_0}{(l_0)^3} \right) = \frac{1}{(m+1)} \frac{1}{1 + 3 \frac{l_p l_0}{l_0 l_p}} \quad (16)$$

In table 1, the results of equations (15) to (16) are compared for different values of the length ratio and parameter m and compared with equation (11), in which all terms are considered (developed code in MATLAB), and FEM using ANSYS.

As seen, the results of equation (15) are very close to the Barillaro *et al* [29] results for the case of the parameter m larger than one; however, for the value of $m = 0$, the difference can reach up to 16%. Additionally, it can be concluded that the results of the current study when all terms are considered, equation (11), are very close to the FEM using computer code, ANSYS, regardless of the value of the parameter m and the ratio of l_p/l_0 . However, the results of equation (15), in which small values of lengths, l_p , are ignored, have deviations from the FEM and equation (11) for small values of the parameter m , and for the case of $m = 0$ (figure 3(a)), the deviation is as high as 37%.

For the case of $\alpha = 0$, using equation (12), the stiffness in the y direction can be calculated. Barillaro *et al* [29] have given the following expression for the calculation of k_y :

$$k_y / \left(\frac{EI_0}{l_0(l_p)^2} \right) = \frac{3(m+1)}{12m^4 + 64m^3 + 130m^2 + 116m + 38} \quad (17)$$

Lu *et al* [30] gave the following equations for the calculation of the stiffness of a serpentine spring in the y direction for the case of $m = 0$, $l_1 = l_2 = 0.5 l_0$:

$$k_y / \left(\frac{EI_0}{l_0(l_p)^2} \right) = \frac{3}{38} \quad (18)$$

which is the same as equation (17) for the case of $m = 0$.

Figure 6 depicts the results of equation (12) for calculation of the stiffness of a horizontal serpentine spring in y direction, which are compared with equation (17) and FEM using computer code ANSYS. For a small value of the parameter m , there are significant differences between the results of the current study and Barillaro *et al* [29]; however, for the parameter m larger than four, the difference is negligible, and the stiffness approaches zero. Additionally, the results of the current study are the same as those of the FEM regardless of the value of the parameter m .

In figure 7, the results of the current study for calculation of the stiffness of an inclined serpentine spring in x direction for the case of $l_1 = l_2 = 0.5 l_0$, $I_{ini} = I_{fin} = I_p = I_0$, $l_{ini} = l_{fin} = l_p = 0.1 l_0$ and $m = 1$ are compared with the FEM for different values of the angle of inclination of the spring, α (figure 1(b)). As seen, there are very good agreements between the results of the present study and FEM.

Comparing table 1 with figure 7, one can conclude that the angle of inclination, α (figure 1(b)) has more effect on the stiffness of a folded-beam spring than the number of folds. In addition, in a restricted area to position a spring, inclining occupied less area than increasing the number of folds.

Figure 8 shows the stiffness of a horizontal serpentine spring with ratios of $l_1 = l_2 = 0.5 l_0$, $I_{ini} = I_{fin} = I_p = I_0$, and $l_p = l_{ini} = l_{fin} = 0.1 l_0$, for different values of the parameter m .

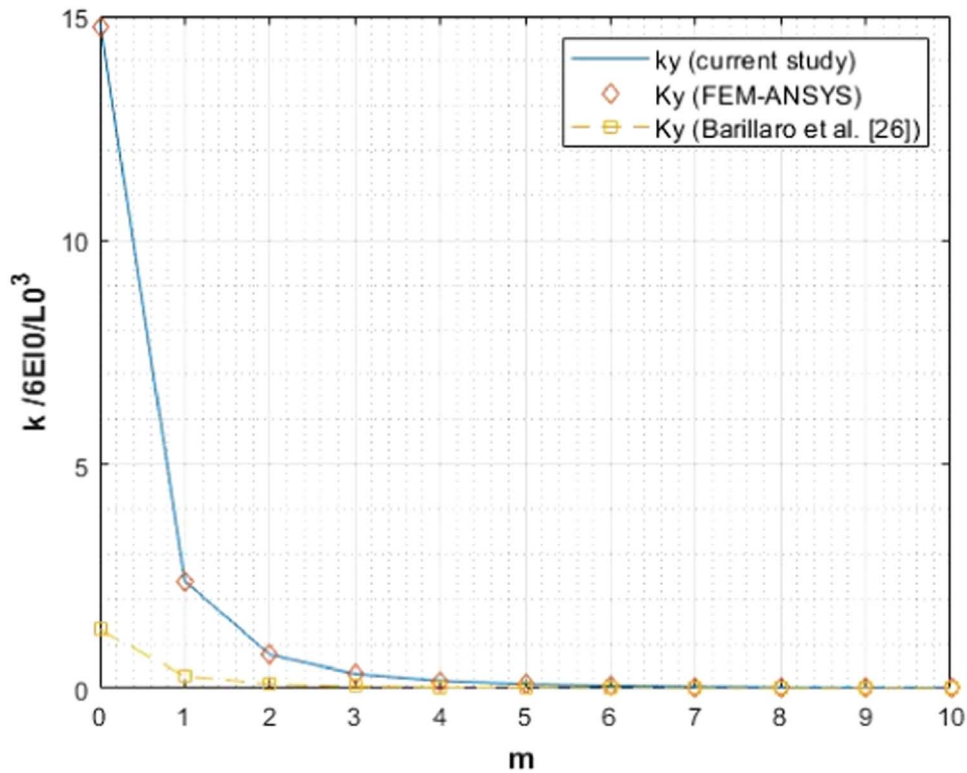


Figure 6. Stiffness of a horizontal serpentine spring in y direction as a function of parameter m, in the case of $l_1 = l_2 = 0.5 l_0$, $I_{ini} = I_{fin} = I_p = I_0$, and $l_{ini} = l_{fin} = l_p = 0.1 l_0$.

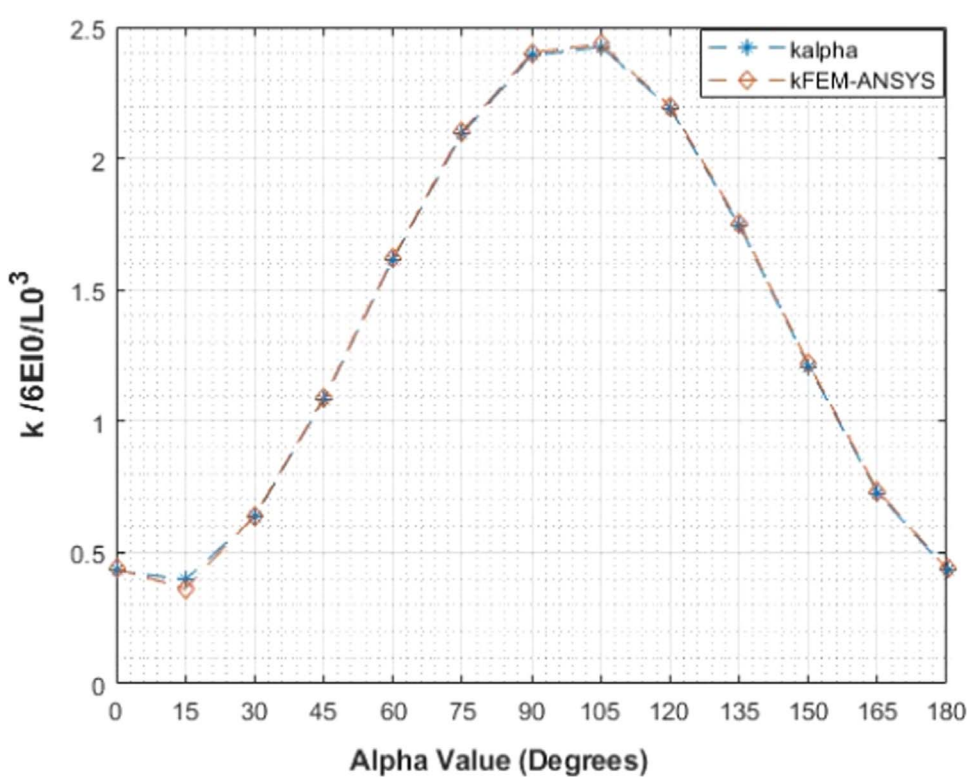


Figure 7. Stiffness of an inclined serpentine spring in x direction with $l_1 = l_2 = \frac{1}{2} l_0$, $I_{ini} = I_{fin} = I_p = I_0$, $l_p = l_{ini} = l_{fin} = 0.1 l_0$, and $m = 1$ for different values of inclination angle.

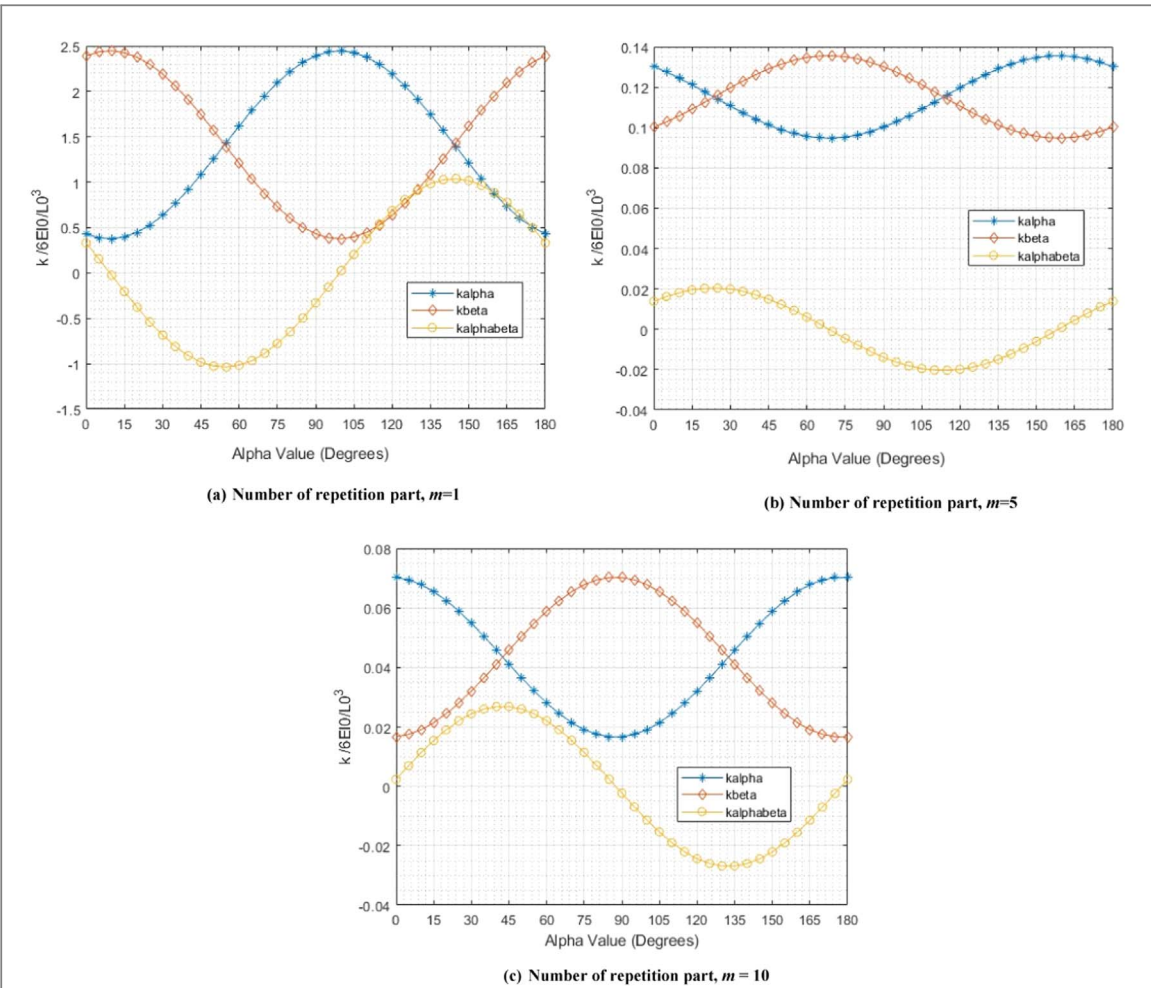


Figure 8. Stiffness of a serpentine spring in two perpendicular directions for the case of ($l_1 = l_2 = 0.5 l_0$, $I_{ini} = I_{fin} = I_p = I_0$, and $l_{ini} = l_{fin} = l_p = 0.1 l_0$).

As seen, the principal axes of the spring constant of a horizontal serpentine spring are different from the x - and y -axes and depend on the geometrical parameters. For example, in the case of $m = 1$, the principal axis of stiffness has an angle of 98 degrees with respect to the x -axis, in which $k_1 = k_\alpha = 2.5(6EI_0/(l_0)^3)$, $k_2 = k_\beta = 0.35(6EI_0/(l_0)^3)$, and $k_{\alpha\beta} = 0$. Having the principal values of stiffness, using equation (3), the stiffness of the spring in any direction can be calculated. For example, spring constants of a horizontal serpentine spring in the direction $\theta = 45^\circ$ with respect to principal axes, are:

$$k_\alpha = k_\beta = \frac{2.5 + 0.35}{2}(6EI_0/(l_0)^3) = 1.425(6EI_0/(l_0)^3)$$

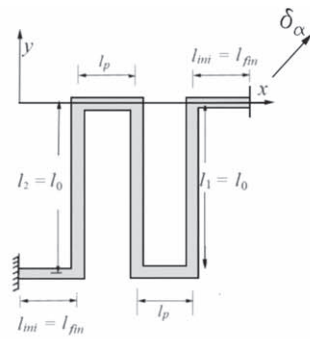
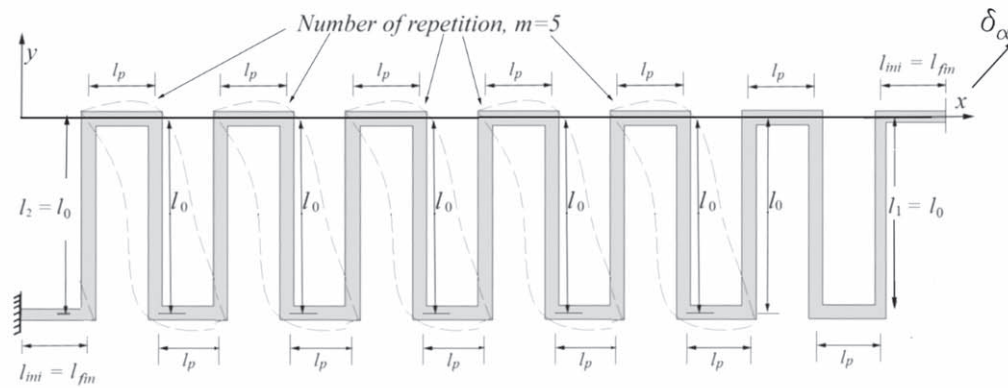
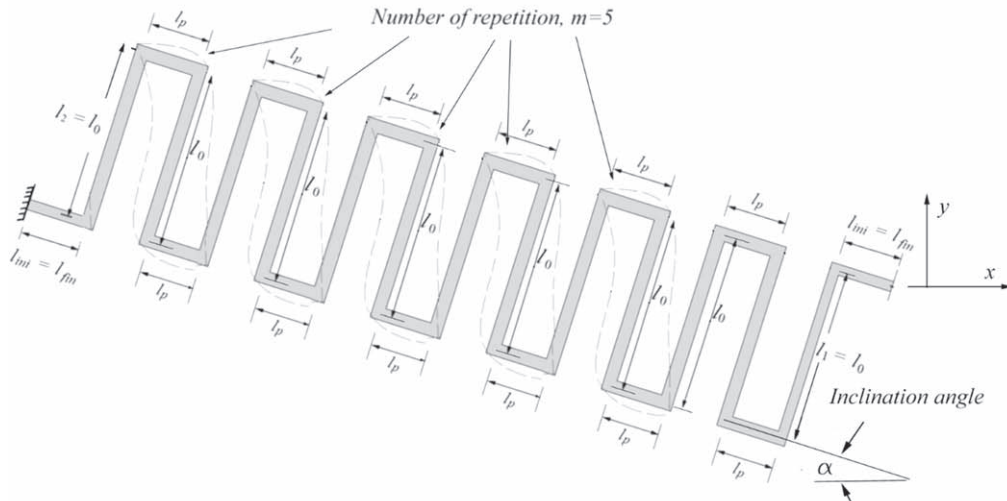
$$k_{\alpha\beta} = \frac{2.5 - 0.35}{2}(6EI_0/(l_0)^3) = 1.075(6EI_0/(l_0)^3)$$

which are the same as the corresponding values for angle $\alpha = 53^\circ$ or $\alpha = 143^\circ$ in figure 8(a). For the case of $m = 5$, the principal axis has rotated approximately 160 degrees with respect to x , and for the case of $m = 10$, the angle is 178 degrees.

4.2. Serpentine spring with length $l_1 = l_2 = l_0$, $I_{ini} = I_{fin}$, and $l_{ini} = l_{fin}$

Fedder [12] calculated the following equations for the determination of k_x and k_y for the case of $l_1 = l_2 = l_0$, $I_{ini} = I_{fin}$ and $l_{ini} = l_{fin}$ (figure 9):

$$k_x / \frac{6EI_0}{(l_0)^3} = \frac{4(m+2)^2 \left(\frac{l_p l_0}{l_0 l_p} + 1 \right) - 6(m+2) + 2}{4(m+2)^3 \left(3 \left(\frac{l_p l_0}{l_0 l_p} \right)^2 + 4 \frac{l_p l_0}{l_0 l_p} + 1 \right) - 4(m+2)^2 \left(5 \frac{l_p l_0}{l_0 l_p} + 2 \right) + (m+2) \left(5 + 6 \frac{l_p l_0}{l_0 l_p} - 9 \left(\frac{l_p l_0}{l_0 l_p} \right)^2 \right) - 1} \quad (19)$$

(a) Horizontal serpentine spring with number of repetitions, m=0 free to displace in α direction(b) Horizontal serpentine spring with number of repetitions, m=5 free to displace in α direction(c) Inclined serpentine spring with number of repetitions, m=5 free to displace in x direction**Figure 9.** Serpentine spring with, $l_1 = l_2 = l_0$, $I_{mi} = I_{fin}$, and $l_{mi} = l_{fin}$.

$$k_y / \frac{6EI_0}{l_0(l_p)^2} = \frac{\frac{3l_p}{l_0} \frac{I_0}{I_p} + 1 - \frac{1}{2(m+2)}}{4(m+2)^3 \left(3 \left(\frac{l_p}{l_0} \frac{I_0}{I_p} \right)^2 + 4 \frac{l_p}{l_0} \frac{I_0}{I_p} + 1 \right) - 4(m+2)^2 \left(5 \frac{l_p}{l_0} \frac{I_0}{I_p} + 2 \right) + (m+2) \left(5 + 6 \frac{l_p}{l_0} \frac{I_0}{I_p} - 9 \left(\frac{l_p}{l_0} \frac{I_0}{I_p} \right)^2 \right) - 1} \quad (20)$$

A computer code in MATLAB is developed based on the equations given in the [appendix](#), and the stiffness of a serpentine spring for the cases of $l_1 = l_2 = l_0$ and $\alpha = 0$ are calculated and compared with equations (19) and (20) ([table 2](#)).

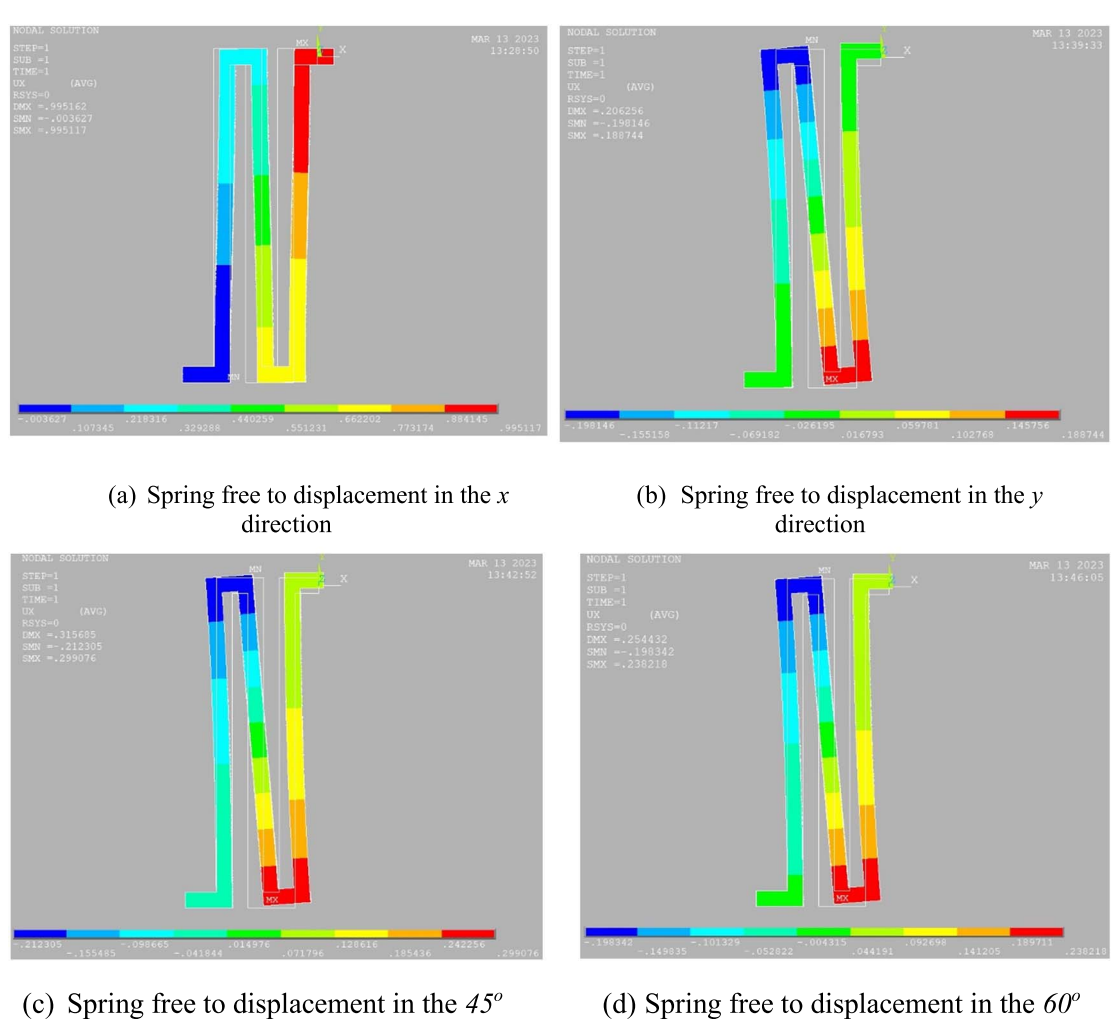


Figure 10. Displacement of a folded-beam spring with $m = 0$, $l_1 = l_2 = l_0$, $I_0 = I_{ini} = I_{fin} = I_p$, and $l_{ini} = l_{fin} = l_p = 0.1 l_0$.

Table 2. Spring constant of serpentine spring in the x direction, for the case of $l_1 = l_2 = l_0$ (figure 9), and $I_{ini} = I_{fin} = I_p = I_0$.

m	$k_x / \frac{6EI_0}{(l_0)^3}$			$k_y / \frac{6EI_0}{(l_0)^3}$		
	Current Study	Fedder [12]	FEM	Current Study	Fedder [12]	FEM
0	0.482	0.482	0.485	6.654	6.654	6.677
1	0.295	0.295	0.299	1.417	1.417	1.424
2	0.213	0.213	0.216	0.517	0.517	0.521
3	0.167	0.167	0.170	0.244	0.244	0.246
4	0.137	0.137	0.140	0.134	0.134	0.135
5	0.116	0.116	0.119	0.081	0.081	0.082
6	0.101	0.101	0.103	0.053	0.053	0.054
7	0.089	0.089	0.091	0.037	0.037	0.037
8	0.080	0.080	0.082	0.026	0.026	0.027
9	0.073	0.072	0.074	0.019	0.019	0.020
10	0.066	0.066	0.068	0.015	0.015	0.015

As seen, the results of the current study are the same as Fedder [12] and have very good agreements with FEM and regardless of the value of the parameter m . Figure 10 shows the displacement of the folded-beam determined using computer code ANSYS for the case of $l_1 = l_2 = l_0$, $I_0 = I_{ini} = I_{fin} = I_p$, $l_{ini} = l_{fin} = l_p = 0.1 l_0$ and $m = 0$ for different values of the angle of inclination of the spring, or the direction that one end of the spring is free to displace.

Figure 11 shows the stiffness of a serpentine spring for the case of $l_1 = l_2 = l_0$ when the parameter m is equal to one and ten.

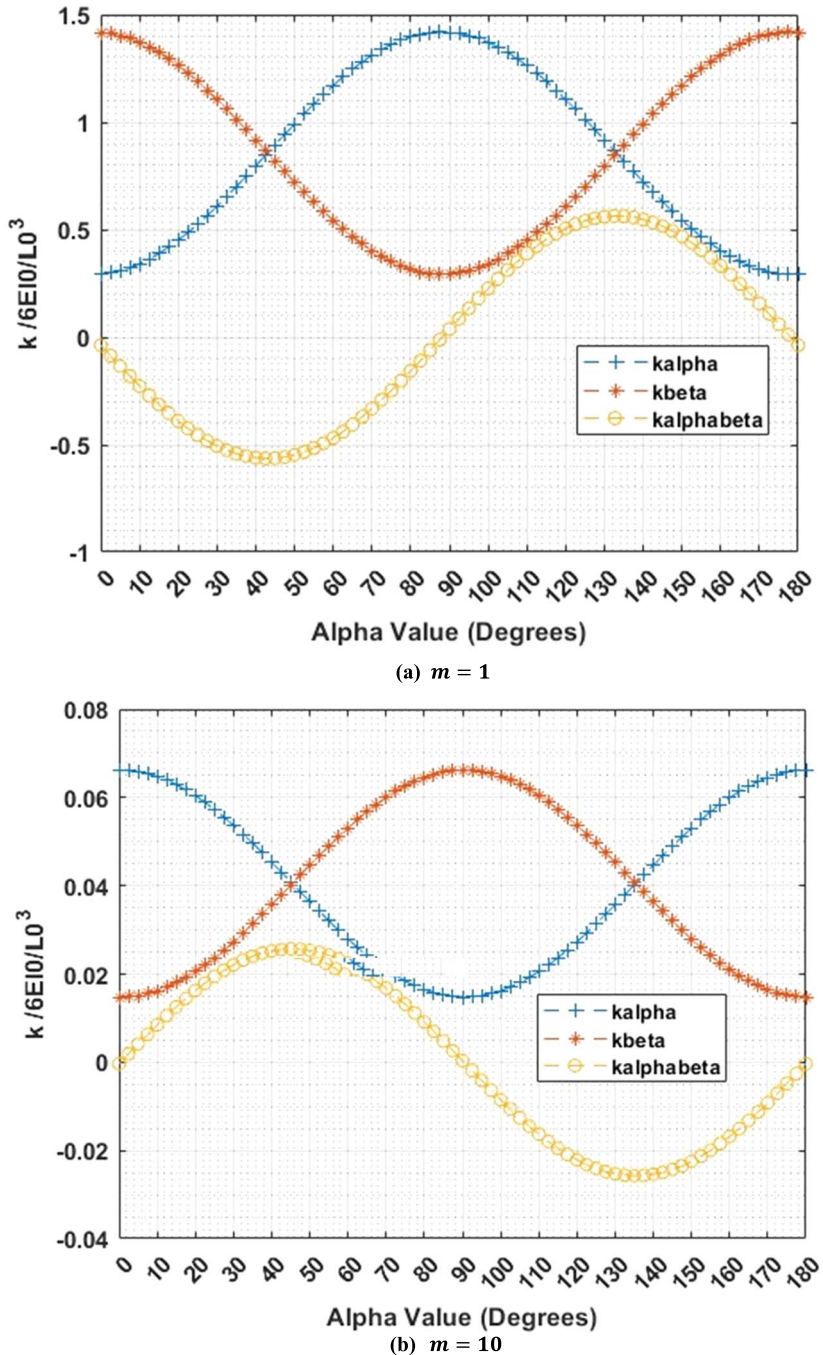


Figure 11. Comparison of stiffness of Serpentine spring in two perpendicular directions for the case of, $l_1 = l_2 = l_0$, and $l_{ini} = l_{fin} = l_p = 0.1 l_0$.

The principal axes of the spring constant in the case of $m = 1$ have an angle of 90 degrees with respect to the x - or y -axes, and for the case of $m = 10$, the principal axis has an angle of zero degrees with respect to the x - and y -axes.

In figure 12, the variation in the angle of the principal axis with respect to the x -axis for different values of the parameter m and two different length ratios of $l_1/l_0 = l_2/l_0$ is depicted. When the parameter m is between zero and three, for the case of $l_1 = l_2 = l_0$ (figure 9), the angle between the principal axis and x -axis is approximately 90 degrees; therefore, the x - and y -axes are principal axes; however, the y -axis corresponds to maximum value of stiffness and x -axis correspond to minimum value of stiffness. For the parameter m larger than five, the angle of the principal axis with respect to the x -axis is zero, which means that the x -axis is the principal axis that has maximum value of stiffness, and the y -axis has minimum value of stiffness. For the case of $l_1 = l_2 = 0.5 l_0$ (figure 3), when the parameter m is less than seven, the x and y -axes are not principal axes, and due to the applied force in the x direction, the spring would displace in both directions of x , and y . However, when the parameter m is

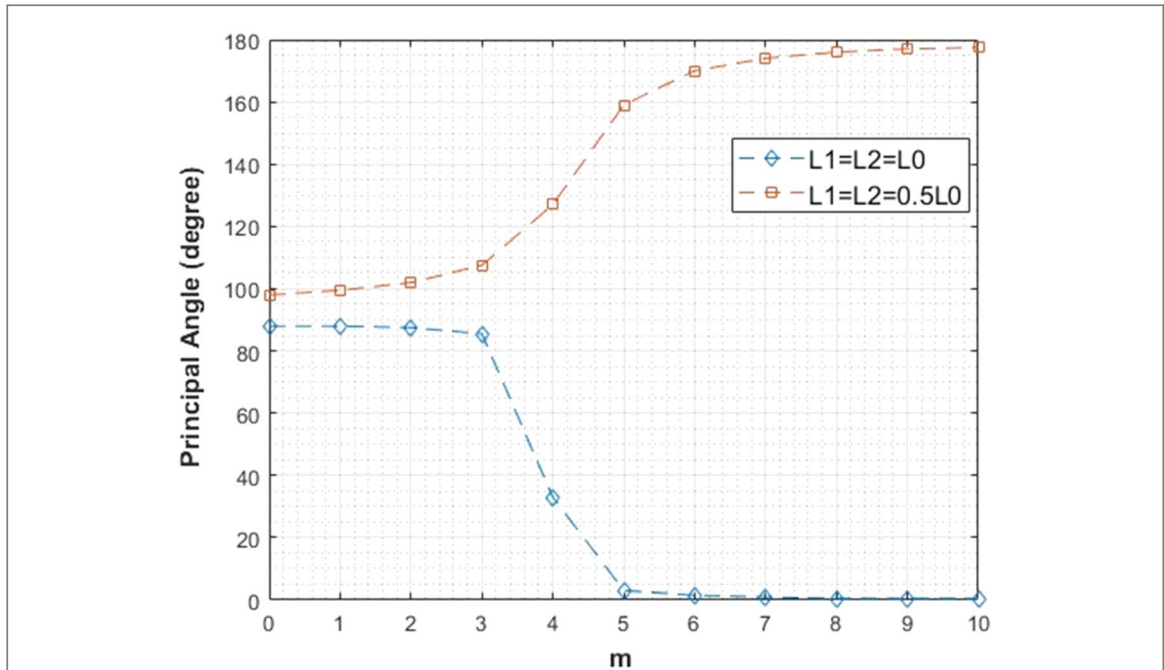


Figure 12. Angle of principal axis in respect to x-axis for different values of parameter m, and $l_{ini} = l_{fin} = l_p = 0.1 l_0$.

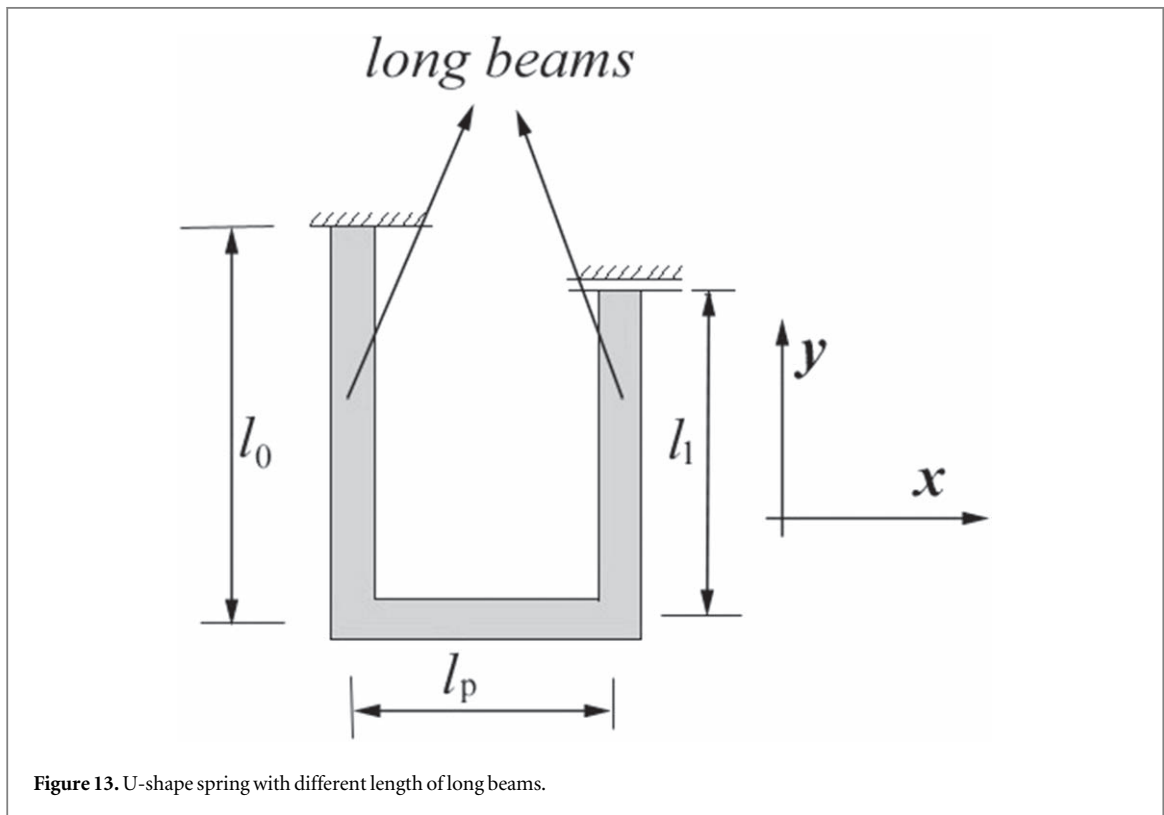


Figure 13. U-shape spring with different length of long beams.

larger than seven, the angle of principal axis with respect to x-axis is 180 degrees. This means that, x is principal axis correspond to maximum value of stiffness, and y-axis correspond to minimum value of stiffness.

4.3. U-shape spring

In a U-shape spring (figure 13), the equations given in the appendix for the calculation of compliance are simplified as follows:

$$\begin{aligned}
C_{\alpha\alpha} \Big/ \frac{(l_0)^3}{EI_0} &= \left(\frac{1}{3} - \frac{l_1}{l_0} + \left(\frac{l_1}{l_0} \right)^2 + \frac{1}{3} \left(\frac{l_1}{l_0} \right)^3 \right) (\cos \alpha)^2 + \frac{l_p}{l_0} \left(\frac{1}{2} - \frac{l_1}{l_0} \right) \sin 2\alpha \\
&+ \left(\frac{l_p}{l_0} \right)^2 (\sin \alpha)^2 + \frac{I_0 l_p}{I_p l_0} \left(\left(\frac{l_1}{l_0} \right)^2 (\cos \alpha)^2 - \frac{1}{2} \frac{l_p}{l_0} \frac{l_1}{l_0} \sin 2\alpha + \frac{1}{3} \left(\frac{l_p}{l_0} \right)^2 (\sin \alpha)^2 \right) \\
C_{\beta\beta} \Big/ \frac{(l_0)^3}{EI_0} &= \left(\frac{1}{3} - \frac{l_1}{l_0} + \left(\frac{l_1}{l_0} \right)^2 + \frac{1}{3} \left(\frac{l_1}{l_0} \right)^3 \right) (\sin \alpha)^2 - \frac{l_p}{l_0} \left(\frac{1}{2} - \frac{l_1}{l_0} \right) \sin 2\alpha \\
&+ \left(\frac{l_p}{l_0} \right)^2 (\cos \alpha)^2 + \frac{I_0 l_p}{I_p l_0} \left(\left(\frac{l_1}{l_0} \right)^2 (\sin \alpha)^2 + \frac{1}{2} \frac{l_p}{l_0} \frac{l_1}{l_0} \sin 2\alpha + \frac{1}{3} \left(\frac{l_p}{l_0} \right)^2 (\cos \alpha)^2 \right) \\
C_{\alpha\beta} \Big/ \frac{(l_0)^3}{EI_0} &= C_{\beta\alpha} \Big/ \frac{(l_0)^3}{EI_0} = \frac{1}{2} \left(\left(\frac{l_p}{l_0} \right)^2 - \frac{1}{3} + \frac{l_1}{l_0} - \left(\frac{l_1}{l_0} \right)^2 - \frac{1}{3} \left(\frac{l_1}{l_0} \right)^3 \right) \sin 2\alpha \\
&+ \frac{l_p}{l_0} \left(\frac{1}{2} - \frac{l_1}{l_0} \right) \cos 2\alpha - \frac{1}{2} \frac{I_0 l_p}{I_p l_0} \left[\frac{l_1}{l_0} \frac{l_p}{l_0} \cos 2\alpha + \left(\left(\frac{l_1}{l_0} \right)^2 - \frac{1}{3} \left(\frac{l_p}{l_0} \right)^2 \right) \sin 2\alpha \right] \\
C_{\alpha\theta} \Big/ \frac{(l_0)^2}{EI_0} &= C_{\theta\alpha} \Big/ \frac{(l_0)^2}{EI_0} = \left(\frac{1}{2} - \frac{l_1}{l_0} - \frac{1}{2} \left(\frac{l_1}{l_0} \right)^2 \right) \cos \alpha + \frac{l_p}{l_0} \sin \alpha + \frac{I_0 l_p}{I_p l_0} \left(\frac{1}{2} \frac{l_p}{l_0} \sin \alpha - \frac{l_1}{l_0} \cos \alpha \right) \\
C_{\beta\theta} \Big/ \frac{(l_0)^2}{EI_0} &= C_{\theta\beta} \Big/ \frac{(l_0)^2}{EI_0} = - \left(\frac{1}{2} - \frac{l_1}{l_0} - \frac{1}{2} \left(\frac{l_1}{l_0} \right)^2 \right) \sin \alpha + \frac{l_p}{l_0} \cos \alpha + \frac{I_0 l_p}{I_p l_0} \left(\frac{1}{2} \frac{l_p}{l_0} \cos \alpha + \frac{l_1}{l_0} \sin \alpha \right) \\
C_{\theta\theta} \Big/ \frac{l_0}{EI_0} &= 1 + \frac{l_1}{l_0} + \frac{I_0 l_p}{I_p l_0}
\end{aligned} \tag{21}$$

Figure 14 depicts the stiffness of the U-shape spring calculated by substituting equation (21) into equations (11) to (13) for different ratios of l_1/l_0 and $I_0 = I_p$.

For the case of $l_1 = l_0$, at $\alpha = 0^\circ$, $k_{\alpha\beta}$ is zero, which means that x and y are principal axes of a U-shape spring with equal length, and since k_β is higher than k_α , thus y -axis correspond to maximum value of stiffness and x -axis correspond to minimum value of stiffness. For the case of $l_1 = 0.5 l_0$, at $\alpha = 3^\circ$, $k_{\alpha\beta}$ is zero; thus, the principal axes have rotated by three degrees with respect to the x - and y -axes. Iyer *et al* [28] determined the cross-axis stiffness of a U-shape spring when l_0 is close to l_1 as follows:

$$k_{xy} = \frac{3EI_p(l_0 - l_1)}{l_p(l_0)^3} \tag{22}$$

Figure 15 depicts the cross-axis stiffness of a U-shape spring calculated by substituting equation (21) in equation (13) as a function of l_1/l_0 for the case of $I_p = I_0$ and compared with equation (22). As seen, for the ratio of l_1/l_0 near one, both equations yield the same results.

For the case of a U-shape spring in which $l_1 = l_0$ (figure 13), substituting equation (21) into equations (11) to (13) for the case of $\alpha = 0^\circ$ yields the stiffness of the U-shape spring with equal length of long beams as follows:

$$k_x \Big/ \frac{6EI_0}{(l_0)^3} = \frac{1 + \frac{1}{2} \frac{I_0 l_p}{I_p l_0}}{1 + 2 \frac{I_0 l_p}{I_p l_0}} \tag{23}$$

$$\begin{aligned}
k_y \Big/ \frac{6EI_0}{(l_0)^3} &= \frac{1}{3} \left(\frac{l_p}{l_0} \right)^2 \left(1 + \frac{1}{6} \frac{I_0 l_p}{I_p l_0} \right) \\
k_{xy} &= 0
\end{aligned} \tag{24}$$

As mentioned earlier, for U-spring with equal length of long beams, the x - and y -axes are principal axes of stiffness; thus, the cross-axis stiffness, k_{xy} , is zero.

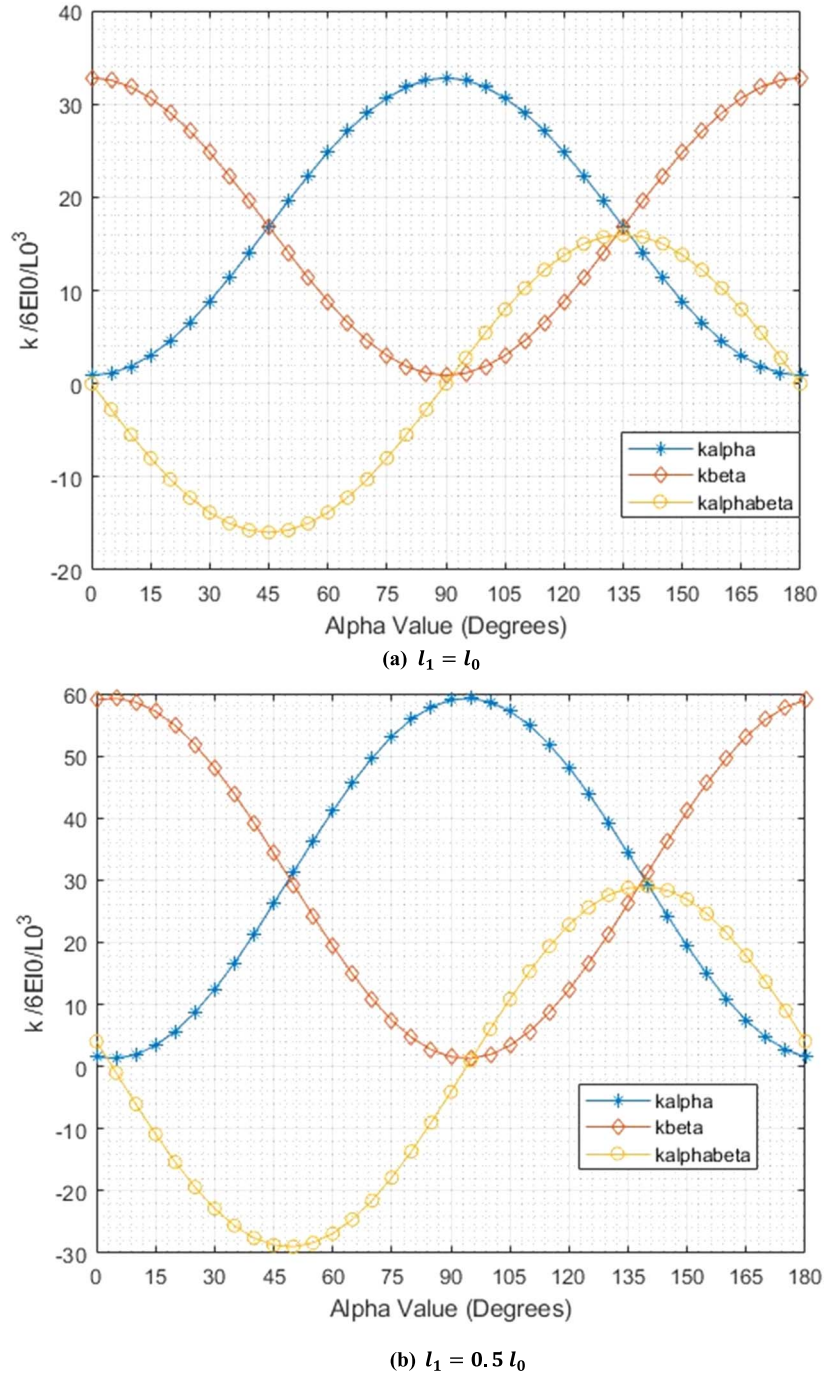


Figure 14. Stiffness of a U-shape spring as a function of inclination angle of spring, α ?($I_p = I_0$).

Wai-Chi et al [31] proposed following equation for calculating the stiffness of a folded-beam in the form of a U-shape spring with equal length in the x direction considering shear deformation:

$$\frac{1}{k_x} = \frac{(l_0)^3}{24EI_0} + \frac{3}{5} \frac{(1 + \mu)l_0}{EhW} + \frac{l_p}{4EA_p} - \frac{l_0(l_p)^2}{16EI_p} \quad (25)$$

where μ is the shear modulus, $A_0 = hW$, and $A_p = h_p W$ are the cross-sectional areas of the beam in longer and shorter beams, respectively. Witter and Howell [32] proposed the following equation for calculation of the stiffness of the same U-spring in the x direction considering shear deformation as well:

$$\frac{1}{k_x} = \frac{1}{WE} \left(\frac{(l_0)^3}{2h^3} + \frac{6}{5}(1 + \mu) \frac{l_0}{h} + \frac{l_p}{2h_p} + \frac{3}{2} \frac{(l_0)^2 l_p}{(h_p)^3} \right) \quad (26)$$

Figure 16 shows the results of equations (23), and (26), which are compared with the FEM.

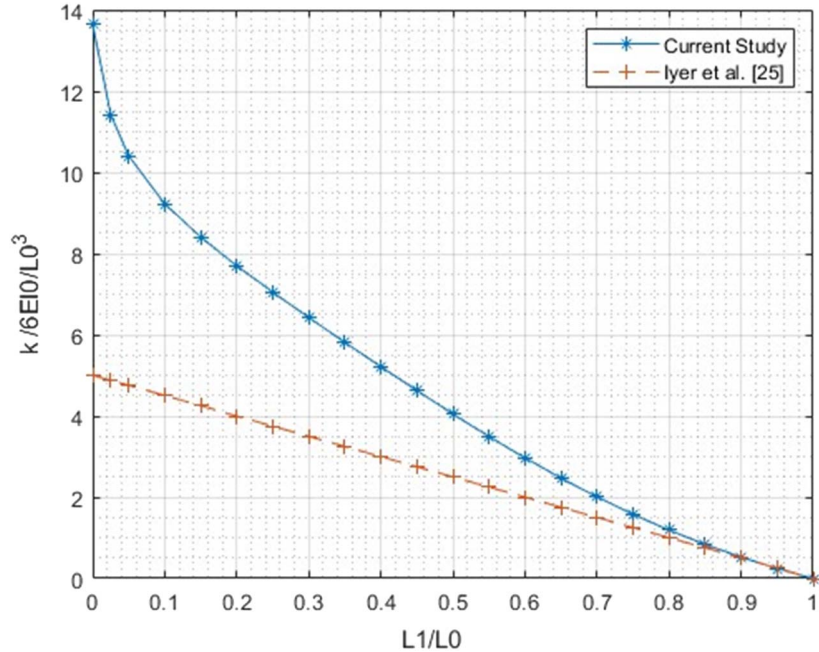


Figure 15. Cross-axis stiffness of a U-shape spring as a function of ratio of length of long beams ($I_0 = I_p$).

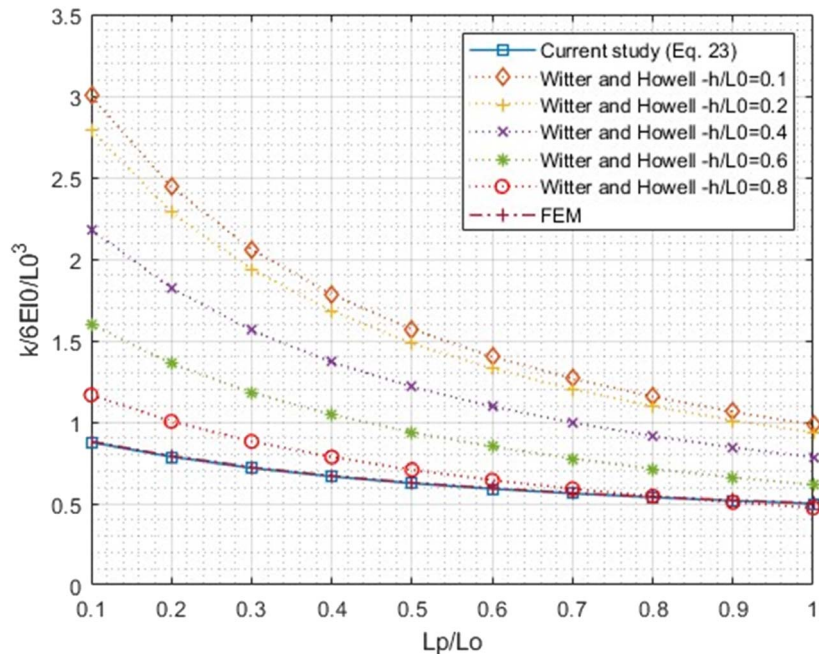


Figure 16. Stiffness of U-shape spring as a function of l_p / l_0 , for the case of $I_0 = I_p$.

As seen, the results of equation (23) and FEM are the same regardless of the ratio of l_p / l_0 , and the results of equation (26) are higher than equation (23). However, as the length of the short beam and/or its height increase, the results of equation (26) approach to the results of equation (23). The results of equation (25) are excluded because it yields a negative value for a large value of the ratio of l_p / l_0 . It worth to mention that figure 16 also valid for the case of $l_p = 0.1 l_0$ and the ratio of I_p / I_0 varies from 1.0 to 10.

Liu and Wu [49] proposed following equation for calculating stiffness of a U-shape beam called single-stage folded-beam, by neglecting the short beam and difference between length of two long beams:

$$k_x = \frac{E(w_0)^3 h}{2(l_0)^3} \quad (27)$$

where,

Table 3. Spring constant of U-shape beam spring in the x direction, $k_x / \frac{6EI_0}{(l_0)^3}$.

Geometrical Parameter	Method	l_1/l_0		
		0.90	1.0	1.10
$\frac{l_p}{l_0} = 0.1$	Current study	1.007	0.875	0.756
	Liu and Wu [49]	1.0	1.0	1.0
$\frac{l_p}{l_0} = 0.05$	Current study	1.075	0.932	0.802
	Liu and Wu [49]	1.0	1.0	1.0
$\frac{l_p}{l_0} = 0.01$	Current study	1.139	0.985	0.846
	Liu and Wen [49]	1.0	1.0	1.0

w_0 is the width of long beam, and h is the height of long beam (figure 13). Table 3 compare the stiffness of a U-shape beam spring calculated by equation (27) and current study.

As seen, when the ratio l_1/l_0 approaches to one, and l_p/l_0 approaches to zero, the results of current study and Liu and Wen [49] are very close, however for the case of $l_1 = 1.10 l_0$, and $l_p = 0.10 l_0$ the deviation is about 25%.

4.4. Crab length spring

Crab length springs consist of two perpendicular beams (figure 17).

Figure 18 depicts the stiffness of a crab length spring as a function of inclination angle, α . When the crab length spring is mounted parallel to the y -axis, its cross-axis stiffness and stiffness in the x -direction are almost zero, and the stiffness in the y -direction is maximum.

For the case of $\alpha = 0$, by substituting equation (21) for the case of $l_1 = 0$ in equations (11) to (13), the stiffness in x , y and cross-axis are determined as follows:

$$k_x / \frac{6EI_0}{(l_0)^3} = \frac{1}{2} \frac{4 + \frac{I_0 l_p}{I_p l_0}}{1 + \frac{I_0 l_p}{I_p l_0}} \quad (28)$$

$$k_y / \frac{6EI_0}{(l_0)^3} = \frac{1}{2} \frac{1 + 4 \frac{I_0 l_p}{I_p l_0}}{\frac{I_0}{I_p} \left(\frac{l_p}{l_0} \right)^3 \left(\frac{I_0 l_p}{I_p l_0} + 1 \right)} \quad (29)$$

$$k_{xy} / \frac{6EI_0}{(l_0)^3} = \frac{3}{2} \frac{1}{l_p \left(1 + \frac{I_0 l_p}{I_p l_0} \right)} \quad (30)$$

Fedder [12] gave the following equations for the calculation of the stiffness of a crab length spring in the x - and y -directions, which are the same as equations (28) and (29):

$$k_x = \frac{3EI_0}{(l_0)^3} \frac{4l_0 + \frac{I_0 l_p}{I_p}}{l_0 + \frac{I_0 l_p}{I_p}}$$

$$k_y = \frac{3EI_p}{(l_p)^3} \frac{4l_0 + \frac{I_0 l_p}{I_p}}{l_0 + \frac{I_0 l_p}{I_p}}$$

Iyer et al [28] gave the following equation for the calculation of the cross-axis stiffness of a crab-length spring, which is the same as equation (30):

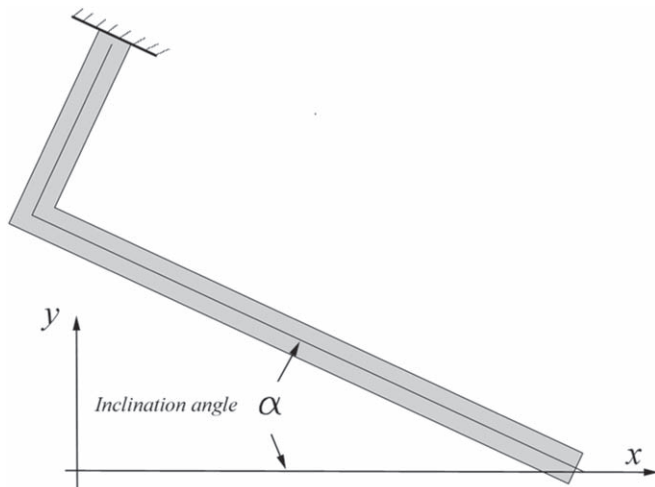


Figure 17. An incline Crab length spring.

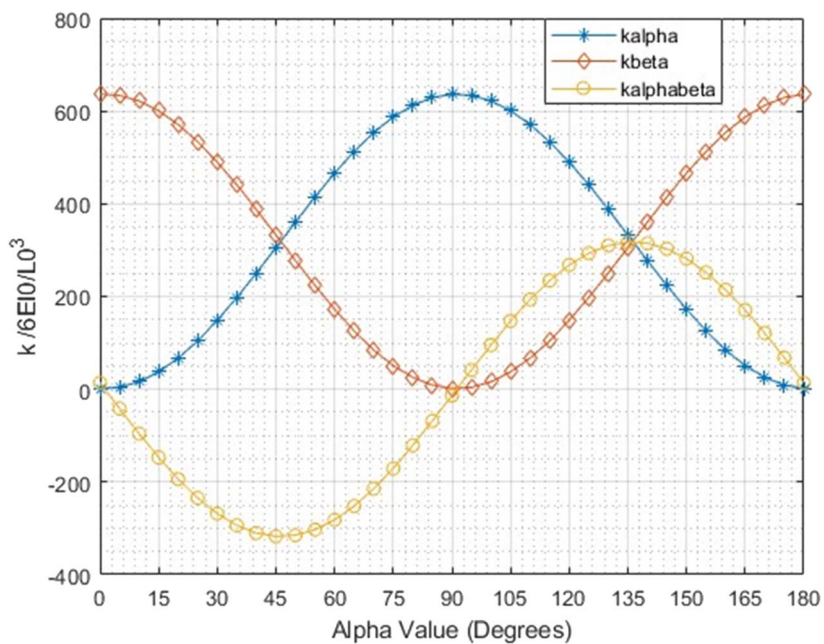


Figure 18. Stiffness of a crab-length spring as a function of inclination angle of spring, α

$$k_{xy} = \frac{9EI_0I_p}{l_0l_p(I_p l_0 + I_0 l_p)}$$

4.5. Serpentine spring with, $l_1 = l_0$, $l_2 = 0$, $l_{ini} = l_p$ and $l_{fin} = 0$

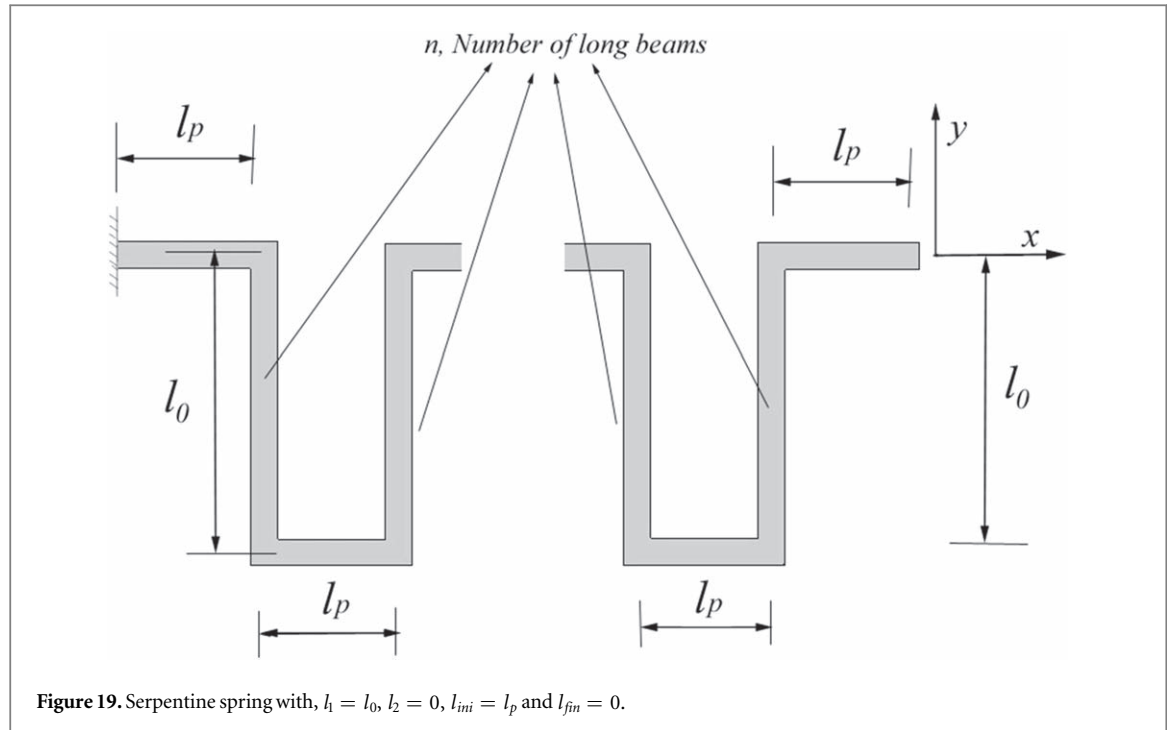
Liu and Wen [33] proposed following equation for calculation of stiffness of a folded-beam spring with, $l_1 = l_0$, $l_2 = 0$, $l_{ini} = l_p$ and $l_{fin} = 0$ (figure 19) in the x direction for the case of $I_0 = I_p$, and neglecting the effect of short beams (l_p) as follows:

$$k_x = \frac{EtW^3}{nL^3} \quad (31)$$

where n is number of long beams, which is equal to $2m + 2$ in figure 1, t and W are thickness and width of the cross section of the beam.

Table 4 depicts the results of equation (31) and current study using the developed code in MATLAB for the case of $I_0 = I_p$, $l_1 = l_0$, and $l_2 = l_{fin} = 0$.

As seen, the results of current study are very close to in equation (31) when the ratio of l_p/l_0 is very small, as the ratio of l_p/l_0 increases, the deviation increases. For example, for the case of $l_p = 0.1 l_0$, and $m = 10$, there is



more than 30% difference between the result of current study and Liu and Wen [33]. Figure 20 depicts variation of this type of serpentine spring ($l_1 = l_0$, $l_2 = 0$, $l_{ini} = l_p = 0.1 l_0$, $l_{fin} = 0$) as a function of inclination angle of spring, α for the case $m = 0$.

As seen, for this serpentine spring principal axes have angle of about 7.5 degrees in respect to x - and y -axes.

4.6. Serpentine spring with, $l_1 = 0$, $l_2 = l_0$, and $l_{ini} = l_{fin} = 0$

Peroulis *et al* [23] gave following equations for calculation of stiffness of a serpentine spring for the case of $l_1 = 0$, $l_2 = l_0$, and $l_{ini} = l_{fin} = 0$ figure 21:

$$\begin{aligned} S_{1x} &= 4(m+1)^2(l_p)^2 + [4(m+1)^2 - 1](l_0)^2 + 2[4(m+1)^2 + 1]l_0l_p \\ S_{2x} &= 2(m+1)[2(m+1) - 3](l_p)^2 + [4(m+1)^2 - 1](l_0)^2 + [8(m+1)^2 - 6(m+1) - 1]l_0l_p \\ k_x / \frac{2EI_0}{l_0^2} &= \frac{S_{1x}/m + 1}{2\left(l_p + \frac{2}{3}l_0\right)S_{1x} - (l_p + l_0)S_{2x} - 3[2(m+1) + 1]l_p(l_p + l_0)^2} \end{aligned} \quad (32)$$

$$\begin{aligned} S_{1y} &= \{2(m+1)l_p + [2(m+1) + 1]l_0\} \left\{ -\frac{2(m+1) + 1}{2} + \frac{l_p\left(l_p + \frac{2}{3}l_0\right)}{(l_p + l_0)\left(l_p + \frac{1}{3}l_0\right)} \right\} \\ S_{2y} &= [2(m+1) + 1](l_p + l_0) \frac{l_p}{2\left(l_p + \frac{1}{3}l_0\right)} \\ k_y / \frac{EI_0}{l_p^2} &= \frac{1/m + 1}{S_{1y} + S_{2y} + \frac{1}{3}\{8(m+1)^2l_p + [2(m+1) + 1][4(m+1) + 1]l_0\}} \end{aligned} \quad (33)$$

Tables 5 and 6 depict the results of equations (32) and (33) which are compared with current study using the developed code in MATLAB for the case of $I_0 = I_p$, $l_1 = 0$, $l_2 = l_0$, and $l_{ini} = l_{fin} = 0$.

As seen, equation (32) for calculation of stiffness of serpentine spring in the x direction yields the same results as current study, however, there are deviations between the results of equation (33) for calculation of stiffness in the y direction, and current study, and this deviation increases by increasing the ratio of l_p/l_0 and by decreasing number of folds, m . For example, for the case of $l_p = 0.1 l_0$, and $m = 0$, the deviation reaches up to 55%. Figure 22 depicts variation of stiffness of this type of serpentine spring as a function of spring inclination angle, α for the case $m = 0$.

As seen, for this serpentine spring principal axes have 2 degrees in respect to x - and y -axes.

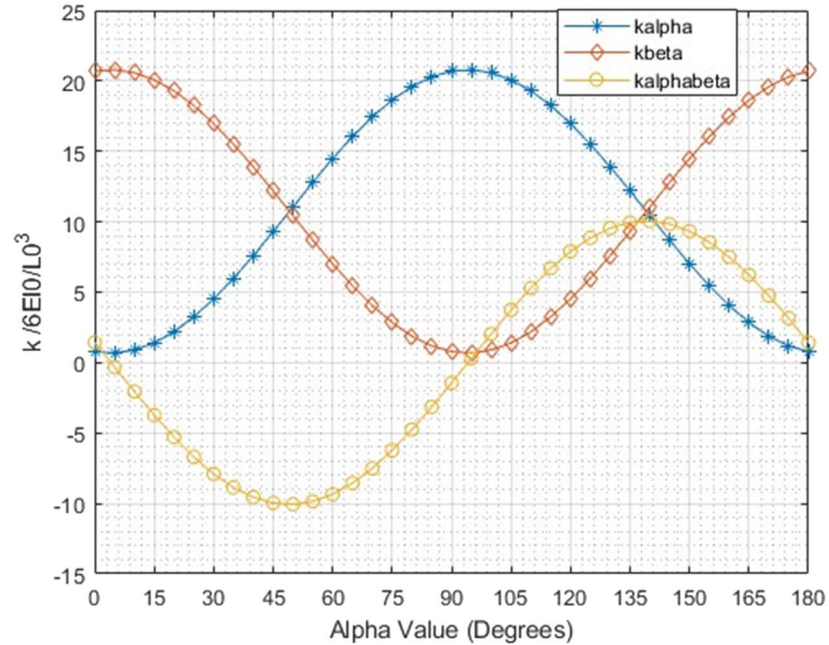


Figure 20. Stiffness of a serpentine spring ($l_1 = l_0$, $l_2 = 0$, $l_{ini} = l_p = 0.1 l_0$, $l_{fin} = 0$) as a function of inclination angle, α for the case of $m = 0$.

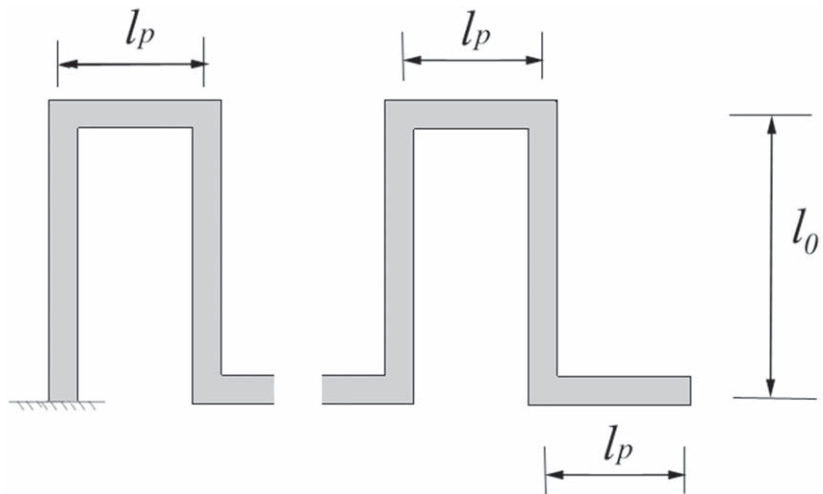


Figure 21. Serpentine spring with, $l_2 = l_0$, $l_1 = 0$, and $l_{ini} = l_{fin} = 0$.

Table 4. Spring constant of folded-beam spring in the x direction, $k_x / \frac{6EI_0}{(l_0)^3}$ for the case of $I_0 = I_p$, $l_1 = l_0$, and $l_2 = l_{fin} = 0$.

Geometrical Parameter	Method	m						
		0	1	2	3	4	5	10
$\frac{l_p}{l_0} = 0.1$	Current study	0.793	0.376	0.250	0.188	0.151	0.126	0.069
	Liu and Wen [33]	1.0	0.5	0.333	0.25	0.2	0.167	0.091
$\frac{l_p}{l_0} = 0.05$	Current study	0.86	0.425	0.285	0.214	0.172	0.144	0.079
	Liu and Wen [33]	1.0	0.5	0.333	0.25	0.2	0.167	0.091
$\frac{l_p}{l_0} = 0.01$	Current study	0.96	0.48	0.322	0.242	0.194	0.161	0.088
	Liu and Wen [33]	1.0	0.5	0.333	0.25	0.2	0.167	0.091

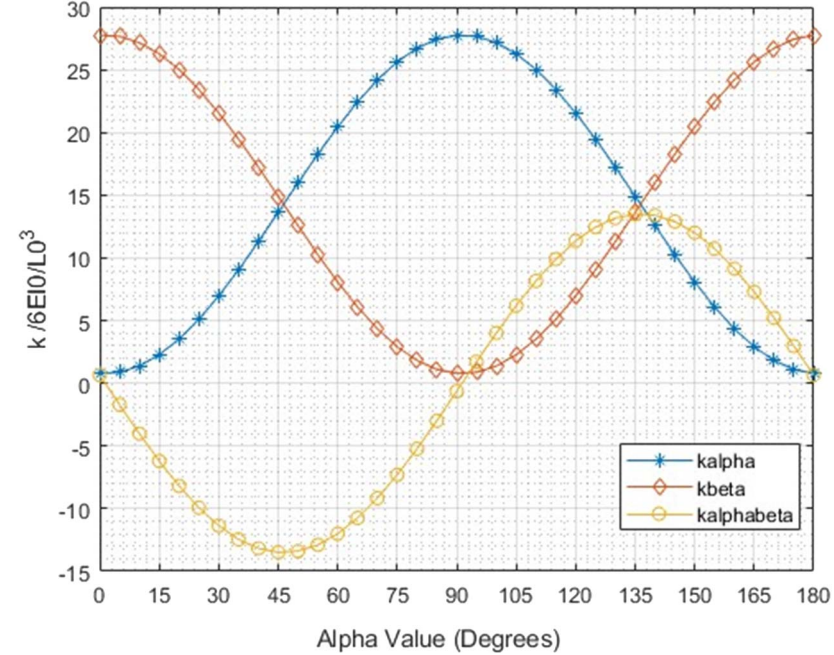


Figure 22. Stiffness of a serpentine spring ($l_1 = 0$, $l_2 = l_0$, $l_{ini} = l_{fin} = 0$) as a function of inclination angle of spring, α for the case of $m = 0$.

Table 5. Spring constant of folded-beam spring in the x direction, $k_x / \frac{6EI_0}{(l_0)^3}$ for the case of $I_0 = I_p$, $l_1 = 0$, $l_2 = l_0$, and $l_{ini} = l_{fin} = 0$ figure 21.

Geometrical Parameter	Method	m						
		0	1	2	3	4	5	10
$\frac{l_p}{l_0} = 0.1$	Current study	0.784	0.386	0.257	0.193	0.154	0.128	0.07
$\frac{l_p}{l_0} = 0.05$	Peroulis <i>et al</i> [23]	0.784	0.386	0.257	0.193	0.154	0.128	0.07
$\frac{l_p}{l_0} = 0.05$	Current study	0.875	0.435	0.290	0.218	0.174	0.145	0.079
$\frac{l_p}{l_0} = 0.01$	Peroulis <i>et al</i> [23]	0.875	0.435	0.290	0.218	0.174	0.145	0.079
$\frac{l_p}{l_0} = 0.01$	Current study	0.971	0.486	0.324	0.243	0.194	0.162	0.088
	Peroulis <i>et al</i> [23]	0.971	0.486	0.324	0.243	0.194	0.162	0.088

Table 6. Spring constant of folded-beam spring in the y direction, $k_y / \frac{6EI_0}{(l_0)^3}$ for the case of $I_0 = I_p$, $l_1 = 0$, $l_2 = l_0$, and $l_{ini} = l_{fin} = 0$.

Geometrical Parameter	Method	m						
		0	1	2	3	4	5	10
$\frac{l_p}{l_0} = 0.1$	Current study	27.751	2.977	0.859	0.359	0.183	0.106	0.017
$\frac{l_p}{l_0} = 0.05$	Peroulis <i>et al</i> [23]	12.236	2.048	0.674	0.300	0.159	0.094	0.016
$\frac{l_p}{l_0} = 0.05$	Current study	120.36	12.56	3.61	1.51	0.768	0.444	0.072
$\frac{l_p}{l_0} = 0.01$	Peroulis <i>et al</i> [23]	69.10	9.98	3.12	1.36	0.707	0.414	0.069
$\frac{l_p}{l_0} = 0.01$	Current study	3258.6	329.19	94.19	39.27	20.00	11.53	1.86
	Peroulis <i>et al</i> [23]	2779.1	311.11	91.01	38.31	19.61	11.36	1.84

5. Conclusion

In this study, a closed-form equation for calculating the stiffness of an inclined folded-beam spring is derived using the energy method. The inclination angle has changed from zero to 180 degrees, and number of folds from zero to ten. First the influence of small lengths in the stiffness of serpentine spring are examined. The results show that for an inclined serpentine spring with an angle between 15 and 165 degrees, neglecting the small lengths of the folded-beam yields inaccurate results. When inclination angle of spring is zero, for calculation of stiffness in the x direction, this neglect is justified only when the number of folded-beams are large. The derived equation is examined against the literature and numerical method using the computer code ANSYS for different types of folded-beam springs including serpentine springs with different length ratio of long and short beams, U-shape springs, and crab-length spring. Mounting the spring in principal axes of spring is crucial in reduction of unwanted parasitic motion, reduction of noise and increasing quality factor. The influential geometrical parameters, including different lengths of short and long beams and inclination angle of the spring on the stiffness are studied, and principal axes of the spring constant are determined. It is found that, the angle of the principal axes of the spring constant depends on the geometrical parameters of the folded-beams. For U-shaped springs, the principal axes are parallel to the beams when the lengths of both long beams are equal. For serpentine springs, the position of the principal axes depends on the number of folded-beams and the ratio of the length short beams to long beams.

Data availability statement

All data that support the findings of this study are included within the article (and any supplementary files).

Appendix

The bending moment at any cross section of the folded-beam spring (figure 23) is defined as:

$$\begin{aligned}
 M_0(x) &= (F_\alpha \sin \alpha + F_\beta \cos \alpha)x + M_\theta \\
 M_1(x) &= (F_\alpha \sin \alpha + F_\beta \cos \alpha)l_{fin} + (-F_\alpha \cos \alpha + F_\beta \sin \alpha)x + M_\theta \\
 M_2(x) &= (F_\alpha \sin \alpha + F_\beta \cos \alpha)(l_{fin} + x) + (-F_\alpha \cos \alpha + F_\beta \sin \alpha)l_1 + M_\theta \\
 M_3(x) &= (F_\alpha \sin \alpha + F_\beta \cos \alpha)(l_{fin} + l_p) + (-F_\alpha \cos \alpha + F_\beta \sin \alpha)(l_1 - x) + M_\theta \\
 M_4(x) &= (F_\alpha \sin \alpha + F_\beta \cos \alpha)(l_{fin} + l_p + x) + (-F_\alpha \cos \alpha + F_\beta \sin \alpha)(l_1 - l_0) + M_\theta \\
 M_5(x) &= (F_\alpha \sin \alpha + F_\beta \cos \alpha)(l_{fin} + 2il_p) + (-F_\alpha \cos \alpha + F_\beta \sin \alpha)(l_1 - l_0 + x) + M_\theta \\
 M_6(x) &= (F_\alpha \sin \alpha + F_\beta \cos \alpha)(l_{fin} + 2il_p + x) + (-F_\alpha \cos \alpha + F_\beta \sin \alpha)l_1 + M_\theta \\
 M_7(x) &= (F_\alpha \sin \alpha + F_\beta \cos \alpha)(l_{fin} + (2i + 1)l_p) + (-F_\alpha \cos \alpha + F_\beta \sin \alpha)(l_1 - x) + M_\theta \\
 M_8(x) &= (F_\alpha \sin \alpha + F_\beta \cos \alpha)(l_{fin} + (2i + 1)l_p + x) + (-F_\alpha \cos \alpha + F_\beta \sin \alpha)(l_1 - l_0) + M_\theta \\
 M_9(x) &= (F_\alpha \sin \alpha + F_\beta \cos \alpha)(l_{fin} + 2(m + 1)l_p) + (-F_\alpha \cos \alpha + F_\beta \sin \alpha)(l_1 - l_0 + x) + M_\theta \\
 M_{11}(x) &= (F_\alpha \sin \alpha + F_\beta \cos \alpha)(l_{fin} + 2(m + 1)l_p + x) + (-F_\alpha \cos \alpha + F_\beta \sin \alpha)(l_2 + l_1 - l_0) + M_\theta
 \end{aligned}$$

Using Castigliano's method, the compliance coefficients are calculated as follows:

$$\begin{aligned}
 C_{\alpha\alpha}/\left(\frac{l_0}{EI_0}\right)^3 &= \left(\frac{1}{3}(2m + 1) - (2m + 1)\frac{l_1}{l_0} + \frac{l_2}{l_0} - 2\frac{l_1 l_2}{l_0 l_0} + (2m + 1)\left(\frac{l_1}{l_0}\right)^2 - \left(\frac{l_2}{l_0}\right)^2 + \frac{1}{3}\left(\frac{l_1}{l_0} + \frac{l_2}{l_0}\right)^3 \right) (\cos \alpha)^2 \\
 &\quad + \left(\frac{1}{2}(2m + 1)\frac{l_{fin}}{l_0} + (m + 1)\left(m + \frac{1}{2}\right)\frac{l_p}{l_0} - (2m + 1)\frac{l_{fin} l_1}{l_0 l_0} + \frac{l_{fin} l_2}{l_0 l_0} - (m + 1)(2m + 1)\frac{l_1 l_p}{l_0 l_0} \right. \\
 &\quad \left. + 2(m + 1)\frac{l_2 l_p}{l_0 l_0} - 2(m + 1)\frac{l_p l_1 l_2}{l_0 l_0 l_0} - \frac{1}{2}\left(\frac{l_1}{l_0} + \frac{l_2}{l_0}\right)^2 \frac{l_{fin}}{l_0} - (m + 1)\left(\frac{l_2}{l_0}\right)^2 \frac{l_p}{l_0} \right) \sin 2\alpha \\
 &\quad + \left(2(m + 1)(2m + 1)\frac{l_{fin} l_p}{l_0 l_0} + (m + 1)\left(\frac{8}{3}m^2 + \frac{10}{3}m + 1\right)\left(\frac{l_p}{l_0}\right)^2 + 4(m + 1)\frac{l_{fin} l_p l_2}{l_0 l_0 l_0} \right. \\
 &\quad \left. + 4(m + 1)^2\left(\frac{l_p}{l_0}\right)^2 \frac{l_2}{l_0} + \left(\frac{l_{fin}}{l_0}\right)^2 \frac{l_1}{l_0} + \left(\frac{l_{fin}}{l_0}\right)^2 \frac{l_2}{l_0} + (2m + 1)\left(\frac{l_{fin}}{l_0}\right)^2 \right) (\sin \alpha)^2
 \end{aligned}$$

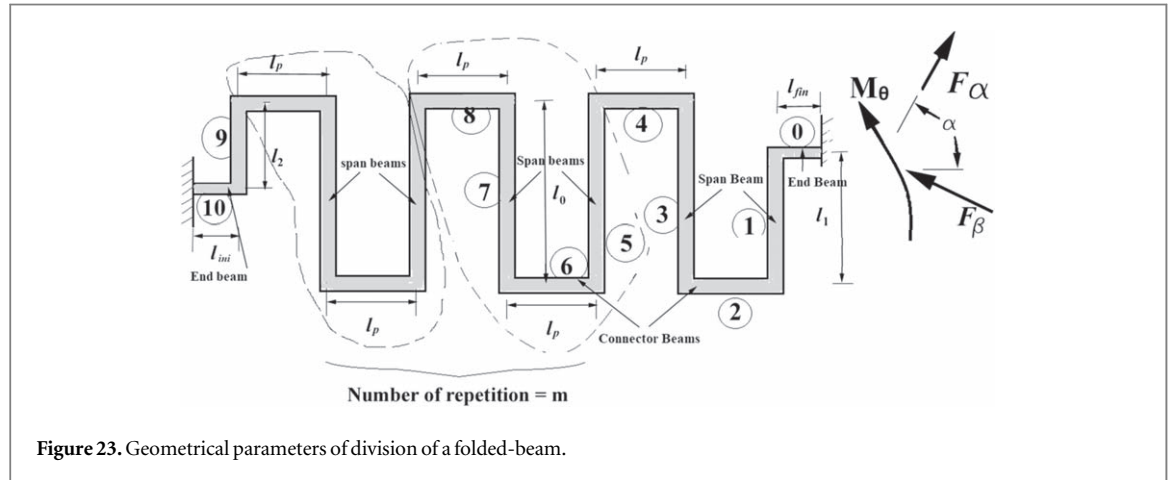


Figure 23. Geometrical parameters of division of a folded-beam.

$$\begin{aligned}
 & + (m+1) \frac{I_0 l_p}{I_p l_0} \left[\left(1 - 2 \frac{l_1}{l_0} + 2 \left(\frac{l_1}{l_0} \right)^2 \right) (\cos \alpha)^2 + \left(\frac{l_{fin}}{l_0} + \left(m + \frac{3}{2} \right) \frac{l_p}{l_0} - 2(m+1) \frac{l_p l_1}{l_0 l_0} - 2 \frac{l_{fin} l_1}{l_0 l_0} \right) \sin 2\alpha \right. \\
 & \quad \left. + 2 \left(\left(\frac{l_{fin}}{l_0} \right)^2 + 2(m+1) \frac{l_p l_{fin}}{l_0 l_0} + \frac{4}{3}(m+1)^2 \left(\frac{l_p}{l_0} \right)^2 \right) (\sin \alpha)^2 \right] + \frac{1}{3} \frac{I_0}{I_{fin}} \left(\frac{l_{fin}}{l_0} \right)^3 (\sin \alpha)^2 \\
 & + \frac{I_0 l_{ini}}{I_{ini} l_0} \left(\left(1 - \frac{l_1}{l_0} - \frac{l_2}{l_0} \right)^2 (\cos \alpha)^2 + \left(\frac{1}{2} \frac{l_{ini}}{l_0} + \frac{l_{fin}}{l_0} + 2(m+1) \frac{l_p}{l_0} \right) \left(1 - \frac{l_2}{l_0} - \frac{l_1}{l_0} \right) \sin 2\alpha \right. \\
 & \quad \left. + \left[\left(\frac{l_{fin}}{l_0} \right)^2 + 4(m+1) \frac{l_p l_{fin}}{l_0 l_0} + 4(m+1)^2 \left(\frac{l_p}{l_0} \right)^2 + \frac{l_{ini} l_{fin}}{l_0 l_0} + 2(m+1) \frac{l_p l_{ini}}{l_0 l_0} + \frac{1}{3} \left(\frac{l_{ini}}{l_0} \right)^2 \right] (\sin \alpha)^2 \right]
 \end{aligned}$$

$$\begin{aligned}
 C_{\alpha\beta} / \frac{(l_0)^3}{EI_0} = C_{\beta\alpha} / \frac{(l_0)^3}{EI_0} = & \left(-\frac{1}{6}(2m+1) + \frac{1}{2}(2m+1) \frac{l_1}{l_0} - \frac{1}{2} \frac{l_2}{l_0} + \frac{l_1 l_2}{l_0 l_0} + (m+1)(2m+1) \frac{l_p l_{fin}}{l_0 l_0} \right. \\
 & + (m+1) \left(\frac{4}{3}m^2 + \frac{5}{3}m + \frac{1}{2} \right) \left(\frac{l_p}{l_0} \right)^2 - \frac{1}{2}(2m+1) \left(\frac{l_1}{l_0} \right)^2 + \frac{1}{2} \left(\frac{l_2}{l_0} \right)^2 + 2(m+1)^2 \left(\frac{l_p}{l_0} \right)^2 \frac{l_2}{l_0} \\
 & - \frac{1}{6} \left(\frac{l_1}{l_0} + \frac{l_2}{l_0} \right)^3 + 2(m+1) \frac{l_{fin} l_p l_2}{l_0 l_0 l_0} + \frac{1}{2} \left(\frac{l_{fin}}{l_0} \right)^2 \left(2m+1 + \frac{l_1}{l_0} + \frac{l_2}{l_0} \right) \sin 2\alpha \\
 & + \left(\frac{1}{2}(2m+1) \frac{l_{fin}}{l_0} + (m+1) \left(m + \frac{1}{2} \right) \frac{l_p}{l_0} - (2m+1) \frac{l_{fin} l_1}{l_0 l_0} + \frac{l_2 l_{fin}}{l_0 l_0} \right. \\
 & \quad \left. - (m+1)(2m+1) \frac{l_1 l_p}{l_0 l_0} + 2(m+1) \frac{l_2 l_p}{l_0 l_0} - \frac{1}{2} \left(\frac{l_1}{l_0} + \frac{l_2}{l_0} \right)^2 \frac{l_{fin}}{l_0} - (m+1) \left(\frac{l_2}{l_0} \right)^2 \frac{l_p}{l_0} \right. \\
 & \quad \left. - 2(m+1) \frac{l_p l_1 l_2}{l_0 l_0 l_0} \right) \cos 2\alpha
 \end{aligned}$$

$$\begin{aligned}
 & + (m+1) \frac{I_0 l_p}{I_p l_0} \left[\left(-\frac{1}{2} + \frac{l_1}{l_0} - \left(\frac{l_1}{l_0} \right)^2 + \left(\frac{l_{fin}}{l_0} \right)^2 + 2(m+1) \frac{l_p l_{fin}}{l_0 l_0} + \frac{4}{3}(m+1)^2 \left(\frac{l_p}{l_0} \right)^2 \right) \sin 2\alpha \right. \\
 & \quad \left. + \left(\frac{l_{fin}}{l_0} + \left(m + \frac{3}{2} \right) \frac{l_p}{l_0} - 2(m+1) \frac{l_p l_1}{l_0 l_0} - 2 \frac{l_{fin} l_1}{l_0 l_0} \right) \cos 2\alpha \right] + \frac{1}{6} \frac{I_0}{I_{fin}} \left(\frac{l_{fin}}{l_0} \right)^3 \sin 2\alpha \\
 & + \frac{I_0 l_{ini}}{I_{ini} l_0} \left\{ \left(\frac{1}{2} \left(\frac{l_{fin}}{l_0} \right)^2 + 2(m+1) \frac{l_p l_{fin}}{l_0 l_0} + 2(m+1)^2 \left(\frac{l_p}{l_0} \right)^2 + \frac{1}{2} \frac{l_{fin} l_{ini}}{l_0 l_0} \right. \right. \\
 & \quad \left. \left. + (m+1) \frac{l_p l_{ini}}{l_0 l_0} + \frac{1}{6} \left(\frac{l_{ini}}{l_0} \right)^2 - \frac{1}{2} \left(1 - \frac{l_1}{l_0} - \frac{l_2}{l_0} \right)^2 \sin 2\alpha \right) \right. \\
 & \quad \left. + \left(\frac{1}{2} \frac{l_{ini}}{l_0} + \frac{l_{fin}}{l_0} + 2(m+1) \frac{l_p}{l_0} \right) \left(1 - \frac{l_1}{l_0} - \frac{l_2}{l_0} \right) \cos 2\alpha \right\}
 \end{aligned}$$

$$\begin{aligned}
C_{\beta\beta}/\frac{(l_0)^3}{EI_0} = & \left(\frac{1}{3}(2m+1) - (2m+1)\frac{l_1}{l_0} + \frac{l_2}{l_0} - 2\frac{l_1}{l_0} + (2m+1)\left(\frac{l_1}{l_0}\right)^2 - \left(\frac{l_2}{l_0}\right)^2\frac{l_2}{l_0} \right. \\
& + \left(\frac{l_1}{l_0}\right)^2\frac{l_2}{l_0} + \left(\frac{l_2}{l_0}\right)^2\frac{l_1}{l_0} + \frac{1}{3}\left(\frac{l_1}{l_0}\right)^3 + \frac{1}{3}\left(\frac{l_2}{l_0}\right)^3 \right) (\sin\alpha)^2 \\
& - \left(\frac{1}{2}(2m+1)\frac{l_{fin}}{l_0} + (m+1)\left(m+\frac{1}{2}\right)\frac{l_p}{l_0} - (2m+1)\frac{l_{fin}l_1}{l_0l_0} + \frac{l_{fin}l_2}{l_0l_0} \right. \\
& - (m+1)(2m+1)\frac{l_1l_p}{l_0l_0} + 2(m+1)\frac{l_2l_p}{l_0l_0} - \frac{l_{fin}l_1l_2}{l_0l_0l_0} - 2(m+1)\frac{l_p l_1l_2}{l_0l_0l_0} \\
& - \frac{1}{2}\left(\frac{l_2}{l_0}\right)^2\frac{l_{fin}}{l_0} - \frac{1}{2}\left(\frac{l_1}{l_0}\right)^2\frac{l_{fin}}{l_0} - (m+1)\left(\frac{l_2}{l_0}\right)^2\frac{l_p}{l_0} \Big) \sin 2\alpha \\
& + \left(2(2m+1)(m+1)\frac{l_{fin}l_p}{l_0l_0} + (m+1)\left(\frac{8}{3}m^2 + \frac{10}{3}m + 1\right)\left(\frac{l_p}{l_0}\right)^2 + 4(m+1)\frac{l_{fin}l_p l_2}{l_0l_0l_0} \right. \\
& + 4(m+1)^2\left(\frac{l_p}{l_0}\right)^2\frac{l_2}{l_0} + \left(\frac{l_{fin}}{l_0}\right)^2\frac{l_1}{l_0} + \left(\frac{l_{fin}}{l_0}\right)^2\frac{l_2}{l_0} + (2m+1)\left(\frac{l_{fin}}{l_0}\right)^2 \Big) (\cos\alpha)^2 \\
& + (m+1)\frac{I_0l_p}{I_pl_0}\left[\left(1 - 2\frac{l_1}{l_0} + 2\left(\frac{l_1}{l_0}\right)^2 \right) (\sin\alpha)^2 - \left(\frac{l_{fin}}{l_0} + \left(m+\frac{3}{2}\right)\frac{l_p}{l_0} - 2(m+1)\frac{l_p l_1}{l_0l_0} - 2\frac{l_{fin}l_1}{l_0l_0} \right) \sin 2\alpha \right. \\
& + 2\left(2(m+1)\frac{l_p l_{fin}}{l_0l_0} + \left(\frac{l_{fin}}{l_0}\right)^2 + \frac{4}{3}(m+1)^2\left(\frac{l_p}{l_0}\right)^2 \right) (\cos\alpha)^2 \Big] + \frac{1}{3}\frac{I_0}{I_{fin}}\left(\frac{l_{fin}}{l_0}\right)^3 (\cos\alpha)^2 \\
& + \frac{I_0l_{ini}}{I_{ini}l_0}\left\{ \left(1 - \frac{l_1}{l_0} - \frac{l_2}{l_0} \right)^2 (\sin\alpha)^2 - \left(\frac{1}{2}\frac{l_{ini}}{l_0} + \frac{l_{fin}}{l_0} + 2(m+1)\frac{l_p}{l_0} \right) \left(1 - \frac{l_1}{l_0} - \frac{l_2}{l_0} \right) \sin 2\alpha \right. \\
& + \left[\left(\frac{l_{fin}}{l_0}\right)^2 + 4(m+1)\frac{l_p l_{fin}}{l_0l_0} + 4(m+1)^2\left(\frac{l_p}{l_0}\right)^2 + \frac{l_{ini}l_{fin}}{l_0l_0} + 2(m+1)\frac{l_p l_{ini}}{l_0l_0} + \frac{1}{3}\left(\frac{l_{ini}}{l_0}\right)^2 \right] (\cos\alpha)^2 \Big\} \\
C_{\theta\alpha}/\frac{(l_0)^2}{EI_0} = C_{\alpha\theta}/\frac{(l_0)^2}{EI_0} = & \left(\frac{1}{2}(2m+1) - (2m+1)\frac{l_1}{l_0} + \frac{l_2}{l_0} - \frac{1}{2}\left(\frac{l_1}{l_0} + \frac{l_2}{l_0}\right)^2 \right) \cos\alpha \\
& + \left((2m+1)\frac{l_{fin}}{l_0} + (2m+1)(m+1)\frac{l_p}{l_0} + \frac{l_1l_{fin}}{l_0l_0} + \frac{l_{fin}l_2}{l_0l_0} + 2(m+1)\frac{l_p l_2}{l_0l_0} \right) \sin\alpha \\
& + (m+1)\frac{I_0l_p}{I_pl_0}\left[2\left(\frac{l_{fin}}{l_0} + (m+1)\frac{l_p}{l_0}\right) \sin\alpha + \left(1 - 2\frac{l_1}{l_0} \right) \cos\alpha \right] + \frac{1}{2}\frac{I_0}{I_{fin}}\left(\frac{l_{fin}}{l_0}\right)^2 \sin\alpha \\
& + \frac{I_0l_{ini}}{I_{ini}l_0}\left\{ \left(\frac{l_{fin}}{l_0} + 2(m+1)\frac{l_p}{l_0} + \frac{1}{2}\frac{l_{ini}}{l_0}\right) \sin\alpha + \left(1 - \frac{l_1}{l_0} - \frac{l_2}{l_0} \right) \cos\alpha \right\} \\
C_{\beta\theta}/\frac{(l_0)^2}{EI_0} = C_{\theta\beta}/\frac{(l_0)^2}{EI_0} = & - \left((2m+1)\left(\frac{1}{2} - \frac{l_1}{l_0}\right) + \frac{l_2}{l_0} - \frac{1}{2}\left(\frac{l_1}{l_0} + \frac{l_2}{l_0}\right)^2 \right) \sin\alpha \\
& + \left(\frac{l_{fin}}{l_0}\left(2m+1 + \frac{l_1}{l_0} + \frac{l_2}{l_0}\right) + (2m+1)\frac{l_p}{l_0}\left(m+1 + \frac{l_2}{l_0}\right) \right) \cos\alpha \\
& + (m+1)\frac{I_0l_p}{I_pl_0}\left[2\left(\frac{l_{fin}}{l_0} + (m+1)\frac{l_p}{l_0}\right) \cos\alpha - \left(1 - 2\frac{l_1}{l_0} \right) \sin\alpha \right] + \frac{1}{2}\frac{I_0}{I_{fin}}\left(\frac{l_{fin}}{l_0}\right)^2 \cos\alpha \\
& + \frac{I_0l_{ini}}{I_{ini}l_0}\left[\left(\frac{l_{fin}}{l_0} + 2(m+1)\frac{l_p}{l_0} + \frac{1}{2}\frac{l_{ini}}{l_0}\right) \cos\alpha - \left(1 - \frac{l_1}{l_0} - \frac{l_2}{l_0} \right) \sin\alpha \right] \\
C_{\theta\theta}/\frac{l_0}{EI_0} = & (2m+1) + \frac{l_1}{l_0} + \frac{l_2}{l_0} + 2(m+1)\frac{I_0l_p}{I_pl_0} + \frac{I_0l_{fin}}{I_{fin}l_0} + \frac{I_0l_{ini}}{I_{ini}l_0}
\end{aligned}$$

ORCID iDs

Ahmad Rahbar Ranji  <https://orcid.org/0000-0002-7056-929X>

References

- [1] Rahbar Ranji A, Damodaran V, Li K, Chen Z, Alirezaei S and Ahamed M J 2022 Recent advances in MEMS-Based 3D hemispherical resonator gyroscope (HRG)—a sensor of choice *Micromachines* **13** 1676
- [2] Lin M-J, Chou H-M and Chen R 2020 Geometric effect on the nonlinear force-displacement relationship of awl-shaped serpentine microsprings for in-plane deformation *materials* **13** 2864
- [3] IEEE Standard for Inertial Sensor Terminology, New York, NY 10017-2394 1994 (USA: IEEE Standards Board)
- [4] Narasimhan V, Li H and Jianmin M 2015 Micromachined high-g accelerometers: a review *J. Micromech. Microeng.* **25** 1–31
- [5] Fedder G K and Jing Q 1999 A hierarchical circuit-level design methodology for microelectromechanical systems *IEEE Trans. Circuits Syst.—II: Analog Digit. Signal Process.* **46** 1309–15
- [6] Yazdi N, Ayazi F and Najafi K 1998 Micromachined inertial sensors *Proc. of the IEEE*
- [7] Sun C-m, Wang C W and Fang W 2008 On the sensitivity improvement of CMOS capacitive accelerometer S. A. A. **141** 347–52
- [8] Gabrielson T B 1993 Mechanical-thermal noise in micromachined acoustic and vibration Sensors *IEEE Transaction on Electron Devices* **40** 903–9
- [9] Yamane D, Konishi T, Safu T, Toshiyoshi H, Sone M, Machida K, Ito H and Masu K 2019 A MEMS Accelerometer for sub-mG Sensing *Sensors Mater.* **31** 2883–94
- [10] Roylance L M and Angell J B 1979 A batch-fabricated silicon accelerometer *IEEE Trans. Electron Devices* **26** 1911–7
- [11] Koberstein L L, Fraga M A and Furlan H 2013 Comparative analysis and simulation of different piezoresistive accelerometer models in *6th ECCOMAS Conf. on Smart Structures and Materials, SMART2013, Politecnico di Torino*
- [12] Fedder G K 1994 *Simulation of Microelectromechanical Systems* University of California at Berkeley
- [13] Qu Z, Liu H, Ouyang H, Hu C and Tu L 2020 A high-sensitivity optical MEMS accelerometer based on SOI double-side micromachining in 2020 *IEEE SENSORS*, (Rotterdam, Netherlands) pp 25–8
- [14] Vladislav A 2006 Theory and design of micromechanical vibratory gyroscopes *MEMS/NEMS Handbook Techniques and Applications* (Boston: Springer) pp 173–94
- [15] Wu X, Xi X, Wu Y and Xiao D 2021 Cylindrical vibratory gyroscope (Singapore: Springer Nature Singapore Pte Ltd)
- [16] Acar C and Shkel A 2009 MEMS vibratory gyroscopes *Structural Approaches to Improve Robustness* (New York, NY 10013, USA: Springer Science+Business Media, LLC)
- [17] Biswas A, Pawar V S, Menon P K, Pal P and Pandey A K 2021 Influence of fabrication tolerances on performance characteristics of a MEMS gyroscope *Microsyst. Technol.* **27** 2679–93
- [18] Khan N and Ahamed M J 2020 Design and development of a MEMS butterfly resonator using synchronizing beam and out of plane actuation *Microsyst. Technol.* **26** 1643–52
- [19] Khan I, Ting D S and Ahamed M J 2021 Design and development of a MEMS vibrating ring resonator with inner rose petal spring supports *Microsyst. Technol.* **27** 985–95
- [20] Wang A, Sahabandabi S, Harrison T, Spicer D and Ahamed M J 2022 Modelling of air damping effect on the performance of encapsulated MEMS resonators *Microsyst. Technol.* **28** 2529–39
- [21] Shkel A, Howe R T and Horowitz R 1999 Modeling and simulation of micromachined gyroscopes in the presence of imperfections in *Int. Conf. on Modeling and Simulation of Microsystems, Puerto Rico*
- [22] Painter C C and Shkel A M 2002 Active structural error suppression in MEMS vibratory gyroscopes in *Proc. of IEEE Sensors (Orlando, FL, USA)*
- [23] Peroulis D, Pacheco S P, Sarabandi K and Katehi L P 2003 Electromechanical Considerations in Developing Low-Voltage RF MEMS Switches *IEEE Trans. Microwave Theory Tech.* **51** 259–70
- [24] Raman R, Shanmuganathan T and Sindhanaiselvi D 2018 Analysis of RF MEMS series switch with serpentine spring shaped cantilever beam for wireless applications *Mater. Today Proc.* **5** 1890–6
- [25] Pacheco S P, Katehi L P and Nguyen C T-C 2000 Design of low actuation voltage RF MEMS switch in *2000 IEEE MTT-S Int. Microwave Symp. Digest (Cat. No.00CH37017) (Boston, MA, USA)*
- [26] Saffari H, Moghadam R A and Koohsorkhi J 2017 Rotated serpentine spring structure for low actuation voltage CPW RF MEMS switch *Micro and Nanosystems* **9** 80–87
- [27] Su G-D J, Hung S H, Jia D and Jiang F 2005 Serpentine spring corner designs for micro-electro-mechanical systems optical switches with large mirror mass *Opt. Rev.* **12** 339–44
- [28] Iyer S, Zhou Y and Mukherjee T 1999 Analytical modeling of cross-axis coupling in micromechanical springs in *Technical Proc. of the 1999 Int. Conf. on Modeling and Simulation of Microsystems (San Juan, PR, USA)*
- [29] Barillaro G, Molfese A, Nannini A and Pieri F 2005 Analysis, simulation and relative performance of two kinds of serpentine springs *J. Micromech. Microeng.* **15** 736–46
- [30] Lu Q, Bai J, Wang K, Chen P, Fang W and Wang C 2018 Single chip-based nano-optomechanical accelerometer based on subwavelength grating pair and rotated serpentine springs *Sensors* **18** 2036
- [31] Wai-Chi W, Azid A A and Majlis B Y 2010 Formulation of stiffness constant and effective mass for a folded beam *Arch. Mech.* **62** 405–18
- [32] Witter J W and Howell L L 2004 Mitigating the effects of local flexibility at the built-in ends of cantilever beams *J. Appl. Mech.* **71** 748–51
- [33] Liu Y-S and Wen K-A 2019 Implementation of a CMOS/MEMS Accelerometer with ASIC Processes *Micromachines* **10** 50
- [34] Urey H, Kan C and Davis W 2005 Vibration mode frequency formulae for micromechanical scanners *J. Micromech. Microeng.* **15** 1713–21
- [35] Kovacs A and Vizvary Z 2001 Structural parameter sensitivity analysis of cantilever- and bridge-type accelerometers S. A. A. **89** 197–205
- [36] Granados-Rojas B, Reyes-Barranca M A, Flores-Nava L M, Abarca-Jiménez G S, Aleman-Arce M A and González-Navarro Y E 2020 On Balanced Tradeoffs between Stiffness and Design Area in CMOS-MEMS Accelerometer Springs in *2020 17th Int. Conf. on Electrical Engineering, Computing Science and Automatic Control (CCE) (Mexico City, Mexico)*
- [37] Jiang K-Y, Chen H-L, Hsu W, Lee Y-K, Miao Y-W, Shieh Y-C and Hung C-Y 2012 A novel suspension design for MEMS sensing device to eliminate planar spring constants mismatch *Sensors* (Taipei, Taiwan: IEEE)
- [38] Xia D, Kong L and Gao H 2015 Design and analysis of a novel fully decoupled tri-axis linear vibratory gyroscope with matched modes *Sensors* **15** 16929–55
- [39] Zhou G and Dowd P 2003 Tilted folded-beam suspension for extending the stable travel range of comb-drive actuators *J. Micromech. Microeng.* **13** 178–83
- [40] Rouabah H A, Gollasch C O and Kraft M 2005 Design optimisation of an electrostatic MEMS actuator with low spring constant for an ‘Atom Chip’ *NSTI-Nanotech 2005* **3** 489–92
- [41] Kaya T, Shiari B, Petsch K and Yates D 2011 Design of a MEMS capacitive comb-drive accelerometer in *COMSOL Conf. (Boston)*

- [42] Petsch K and Kaya T 2012 Design, fabrication, and analysis of MEMS Three-direction capacitive accelerometer in *Proc. of the 2012 ASEE North Central Section Conf. (San Antonio, Texas)*
- [43] Yamane D, Konishi T, Safu T, Toshiyoshi H, Sone M, Masu K and Machida K 2016 A design of spring constant arranged for MEMS accelerometer by multi-layer metal technology in *Proc. of the 11th IEEE Annual Int., Conf. on Nano/Micro Engineered and Molecular Systems (NEMS) (Matsushima Bay and Sendai MEMS City, Japan)*
- [44] Guo T, Wei W, Cai Q, Cui R, Shen C and Cao H 2022 Design and Fabrication of a Novel Wheel-Ring Triaxial Gyroscope Sensors [229978](#)
- [45] Legtenberg R, Groeneveld A W and Elwenspoek M 1996 Comb-drive actuators for large displacements *J. Micromech. Microeng.* **6** 320–9
- [46] Xia D and Xu L 2017 Coupling mechanism analysis and fabrication of triaxial gyroscopes in monolithic MIMU *Micromachines* **8** 310
- [47] Painter C C and Shkel A M 2001 Structural and thermal analysis of a MEMS angular gyroscope in *SPIE's 8th Annual Int. Symp. on Smart Structures and Materials 2001 (Newport Beach, CA, United States)*
- [48] ANSYS, ANSYS (v2022 R1), ANSYS Inc. 2022
- [49] Liu H, Zhang Y and Wu J 2022 Structural design and testing of a micromechanical resonant accelerometer *Micromachines* **13** 1271